

Carbon emissions of durable FRP composite structures in civil engineering

TianQiao Liu^{a,b}, Jun-Tian Tang^c, Shaojie Zhang^c, Li Dong^c, Lili Hu^{d,e}, Xinmiao Meng^f,
Yange Zhao^{c,g}, Peng Feng^{c,*}

^a Chongqing Research Institute of Beijing University of Technology, Chongqing 401121, China

^b State Key Laboratory of Bridge Engineering Safety and Resilience, Beijing University of Technology, Beijing 100124, China

^c MOE Key Lab of Civil Engineering Safety and Durability, Department of Civil Engineering, Tsinghua University, Beijing 100084, China

^d State Key Laboratory of Ocean Engineering, School of Naval Architecture, Ocean and Civil Engineering, Shanghai Jiao Tong University, Shanghai 200240, China

^e Shanghai Key Laboratory for Digital Maintenance of Buildings and Infrastructures, Shanghai Jiao Tong University, Shanghai 200240, China

^f Department of Civil Engineering, Beijing Forestry University, Beijing 100083, China

^g Design Department, China Academy of Building Research, Beijing 100011, China

ARTICLE INFO

Keywords:

Carbon Emissions
FRP Composite Structures
Civil Engineering
FRP Structural Profiles
FRP Rebars
FRP Sheets

ABSTRACT

Conventional structural materials—concrete and steel—have been producing a substantial amount of carbon emissions to the earth, accounting for over 50 % of industrial emissions worldwide. An urgent call has been made for an alternative structural material with a better environmental impact. In this regard, this work investigated the carbon emissions of durable FRP composite structures in civil engineering. Three typical FRP composite structures were focused, including pedestrian bridges constructed by FRP structural profiles, concrete structures reinforced by FRP rebars, and existing concrete and steel structures strengthened by FRP sheets. Carbon emissions were investigated in terms of the carbon footprints per available dataset. Direct carbon reductions were observed in three FRP composite structures, and also, indirect carbon reductions were discussed, including FRP reinforcement for concrete structures and FRP enclosure for houses. The observed carbon reductions realized by FRP composite structures successfully showcased their great potential in reducing the carbon emissions in civil engineering.

1. Introduction

In civil engineering, fiber reinforced polymer (FRP) composites have been increasingly adopted as a competitive alternative to conventional structural materials such as steel and concrete [1]. FRP composites can be manufactured and used in a variety of forms, including sheets, rebars, structural profiles, etc., and generally, they all have high strength- and stiffness-to-weight ratios, excellent corrosion resistance, and superior fatigue performance [2]. Owing to their favorable features, FRP composites have seen successful applications in strengthening of existing structures [3–7], reinforcing of concrete structures [8] and constructing of new structures [9–12]. Compared to typical steel and concrete structures, those structures incorporating FRP composites (referred to as FRP composite structures in this work) are able to achieve an improved structural performance, a prolonged service life, a lighter self-weight, and a reduced cost pertaining to transportation and construction.

Nonetheless, the carbon emissions of FRP composite structures have not been systematically investigated, and in the near future, this issue may become a decisive factor in the field of civil engineering.

Reducing the carbon emissions of civil engineering structures has never been more important and urgent than today. Steel and concrete are the most widely used structural materials worldwide. However, both of their productions involve high energy/carbon-intensive processes such as heating the iron ore and producing the cement [13,14]. In 2019, steel- and cement-making processes generated 2.6 and 2.4 gigaton of CO₂ emissions, respectively, each accounting for 28 % and 26 % of total industrial emissions worldwide [14], and China is responsible for 57 % of world's total cement production [15]. Such a huge amount of carbon emissions should naturally make them high-prior targets for carbon reductions. However, this is often difficult to achieve due to the necessary heating process as well as the inherent chemical reactions [14]. To date, a large number of cement and steel are still needed every year; for

* Corresponding author.

E-mail addresses: liu_tianqiao@bjut.edu.cn (T. Liu), tjt21@mails.tsinghua.edu.cn (J.-T. Tang), zhangsj20@mails.tsinghua.edu.cn (S. Zhang), dl22@mails.tsinghua.edu.cn (L. Dong), lilihu@sjtu.edu.cn (L. Hu), mengxinmiao@bjfu.edu.cn (X. Meng), zhaoyg@cabr-design.com (Y. Zhao), fengpeng@tsinghua.edu.cn (P. Feng).

<https://doi.org/10.1016/j.engstruct.2024.118482>

Received 17 November 2023; Received in revised form 15 April 2024; Accepted 18 June 2024

Available online 27 June 2024

0141-0296/© 2024 Elsevier Ltd. All rights reserved, including those for text and data mining, AI training, and similar technologies.

Table 1
Embodied CO₂ emissions of FRP composites, steel, and concrete reported in literature.

Authors	Embodied CO ₂ emissions of FRP composites (kg CO ₂ eq./kg)	
	Material identifications	Values
Daniel[23]	Composite	0.50
Tanaka et al. [24]	GFRP (hand layup profile)	4.97
	GFRP (pultruded profile)	3.09
Zhang et al. [43]	GFRP	8.10
	Epoxy resin	5.91
Mara and Haghani[26]	GFRP	5.00
Li et al. [28]	Glass fiber	2.63
	Epoxy resin	6.72
Zubail et al.[32]	E-glass fiber	1.77
	Carbon fiber	15.6
	Epoxy resin	5.90
Authors	Embodied CO ₂ emissions of steel (kg CO ₂ eq./kg)	
	Material identifications	Values
Daniel[23]	Struct. steel	0.33
Tanaka et al. [24]	Steel rebar	0.76
	Steel pile	1.25
	PC tendon	1.31
	Galvanized steel	2.82
Zhang et al. [43]	Steel rebar	1.71
	Steel	1.77
Mara and Haghani[26]	Reinforcement steel	1.71
Li et al. [28]	Reinforcement	1.45
	Steel section	1.77
Zubail et al.[32]	Carbon steel	1.05
Authors	Embodied CO ₂ emissions of concrete (kg CO ₂ eq./kg)	
	Material identifications	Values
Daniel[23]	Concrete	0.20
Tanaka et al. [24]	Concrete ($f_c = 27$ MPa)	0.08
Zhang et al. [43]	Concrete (general)	0.13
Mara and Haghani[26]	Prefabricated concrete	0.22
Li et al. [28]	Concrete	0.21

Table 2
Embodied CO₂ emissions of FRP composites, steel, and concrete reported in database.

Sources	Embodied CO ₂ emissions (kg CO ₂ eq./kg)	
	Material identifications	Values
ICE[41]	GFRP	8.10
	Epoxide resin	5.70
	Fiberglass	1.54
	Steel (general)	1.95
	Bar and rod	1.86
	Pipe	1.94
	Plate	2.21
	Section	2.03
	Stainless	6.15
	Concrete (general)	0.11
	Aggregate	0.005
	Cement	0.95
	CEE[42]	Pultruded GFRP (I-Beam)
Pultruded GFRP (cross-arm)		0.57
Moulded fiberglass		0.79
CFRP		10.09
GB/T-51366[44]	PU hard foam plate	5.22
	Plain carbon steel (general)	2.05
	Hot-rolled carbon steel section (small)	2.31
	Hot-rolled carbon steel rebar	2.34
	Hot-rolled carbon steel rod	2.34
	Hot-rolled carbon steel plate (medium)	2.40
	Hot-rolled carbon steel seamless pipe	3.15
	Concrete (C30)	0.12
	Concrete (C50)	0.15
	Cement (general)	0.74
	Sand ($f=1.6-3.0$)	0.0025
Aggregate ($d=10-30$ mm)	0.0022	

instance, in 2021, the world's cement production has reached 23.6 gigaton [16].

In this regard, Kyoto Protocol [17] prescribes the reduction targets of carbon emissions for 37 industrialized countries when first adopted in 1997 and has been further expanded to 192 counties/parties as of today. Recently, Chinese government promulgated a national strategy called 'Carbon Peak and Carbon Neutralization' and announced that the carbon emissions nationwide are to reach the peak by 2030 and to achieve the neutralization by 2060 [18]. Civil engineering, as one of the highest carbon-intensive engineering sectors, has been highlighted by many governments that dramatic actions/policies must be implemented so as to reduce the carbon emissions that occurred at every stage of the industry, including material manufacturing, transportation, construction, maintenance, and end-of-life decommissioning.

In this work, carbon emissions of typical FRP composite structures are investigated, and carbon reductions realized by FRP composites are compared with their concrete and steel counterparts. The organization of this work is as follows. First, a literature review was conducted to explore the possible carbon reductions achieved by FRP composite structures as well as the existing methods for calculating the carbon emissions. Second, three typical FRP composite structures in civil engineering are designed, including pultruded FRP pedestrian bridges, FRP rebar-reinforced concrete structures and FRP sheet-strengthened existing structures. Third, carbon emissions of the designed structures were analyzed. Then, discussions were provided regarding the findings obtained from this work and the recommendations for future work. Finally, conclusions drawn from this work were presented.

2. Literature review

2.1. FRP composite structures in civil engineering

FRP pedestrian bridges have seen successful applications in many countries [19–21] and now, they have shown great potential in reducing carbon emissions [22]. A bridge superstructure replacement project in Netherlands demonstrated the lower carbon emissions of FRP composites over structural steel and concrete [23]. Another pedestrian bridge in Okiwana, Japan also showcased that FRP composites produced less CO₂ emissions (in total, by 26 %) as compared to prestressed concrete bridge [24,25]; that is, a smaller substructure was needed to support the lighter FRP superstructure. Owing to the lighter weight, less construction- and transportation-related CO₂ emissions are produced. Moreover, the lighter weight of FRP composites is also favored in rehabilitating the old bridges. For instance, replacing the deteriorated concrete deck by FRP deck was seen to produce less CO₂ emissions [26,27]. On the other hand, the good environmental durability of FRP composites also has a positive impact in reducing the CO₂ emissions of FRP bridges. For instance, the high-saline condition near sea/ocean might require special anti-corrosion measures for concrete and steel bridges, thus leading to higher carbon emissions, while this is not the case for FRP bridges [28].

In addition, using glass- and carbon-fiber (denoted as GFRP and CFRP, respectively) sheets to strengthen the existing concrete beams could permit a substantial amount of CO₂ emission reductions, by 76 % and 69 %, respectively, as compared to replacing those beams with new ones [29]. Prolonging the service life of existing structures using relatively small amount of FRPs is expected to greatly promote the sustainability from many aspects [30]. FRP green fence for agricultural purpose could also lead to 34 % reduction of life-cycle CO₂ emissions as compared to steel fence [31]. The reduced carbon emissions were attributed to the zero-maintenance allowed by FRP composites. Moreover, GFRP and CFRP oil pipes can be used to replace the metallic pipes, and CO₂ reductions by up to 60 % were observed [32].

2.2. Material compositions of FRP composites

Thermoplastic CFRPs were found to yield the highest CO₂ emissions

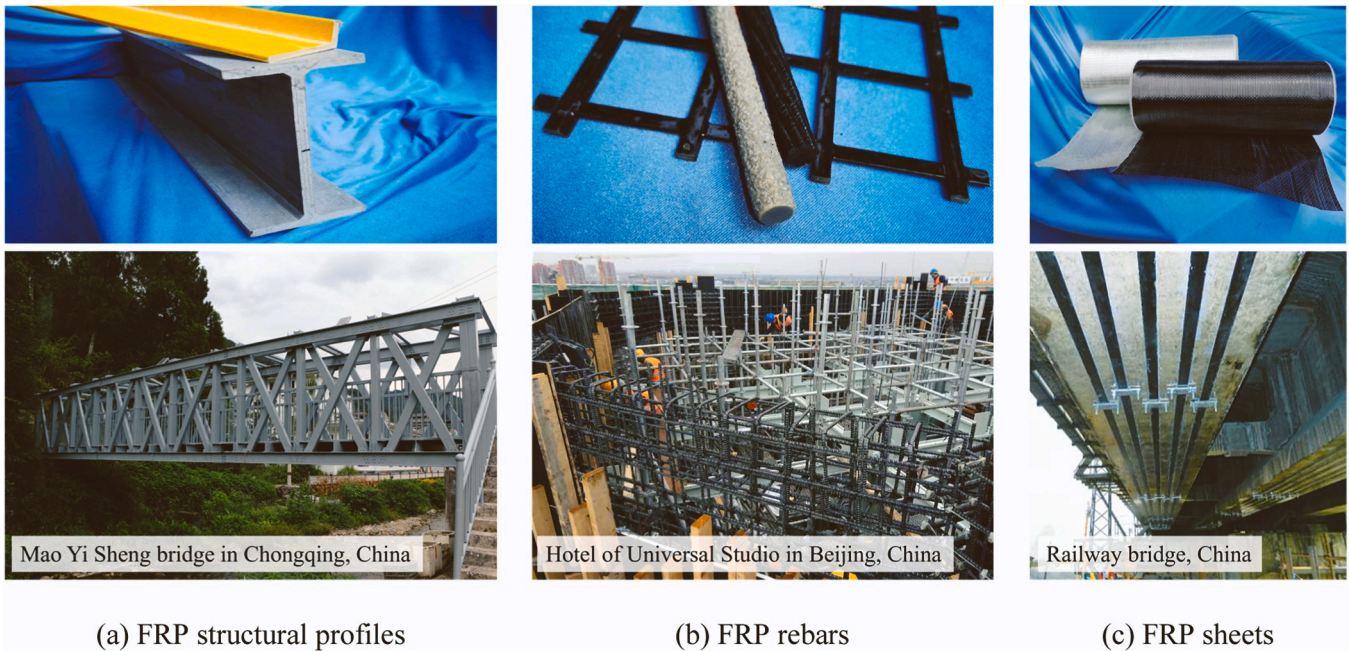


Fig. 1. Typical FRP composites and their applications (a) Pultruded FRP structural profiles are dominantly made of glass fibers, namely GFRP profiles. (b) FRP rebars are made of carbon and glass fibers, and the latter is dominantly used in the field due to the lower cost. (c) FRP sheets are made of carbon and glass fibers and typically in form of fabric. For strengthening of existing structures, CFRP sheets are often preferred over GFRP sheets.

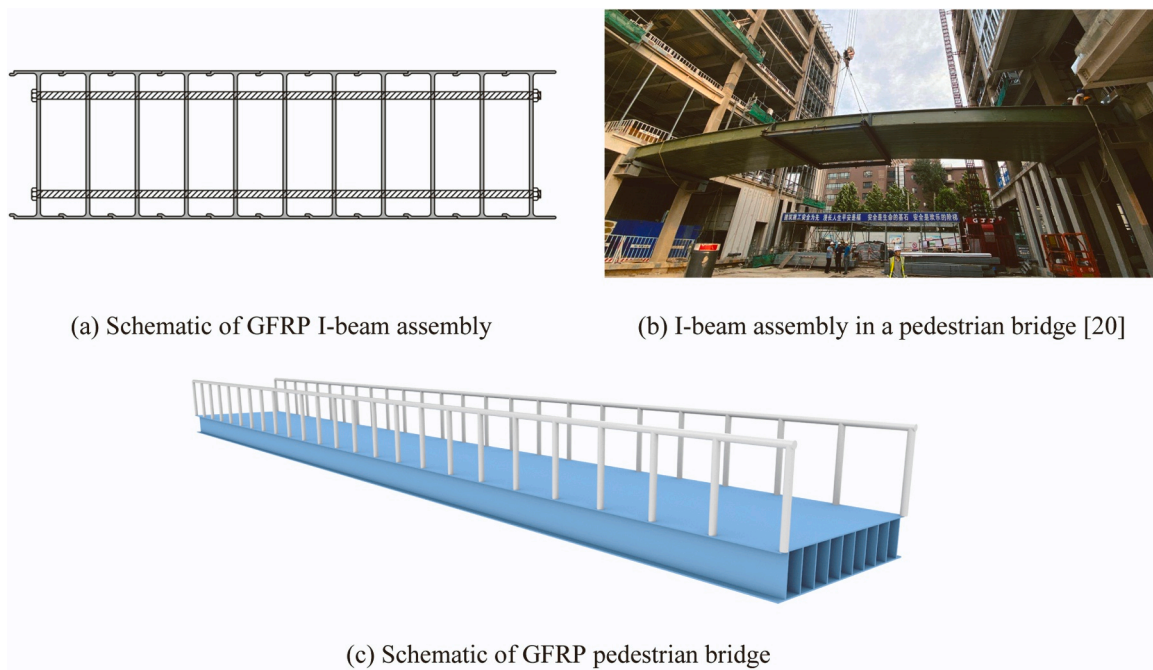


Fig. 2. GFRP pedestrian bridge (a) Eleven I-beams were assembled together by steel rebars to realize the bridge structure. (b) This I-beam assembly was adopted in a 20-m-span pedestrian bridge in 2019, in Beijing, China. (c) In this work, the GFRP pedestrian bridges were designed following the design of I-beam assembly.

as compared to thermoplastic and thermoset GFRPs [32]. As expected, CFRPs resulted in higher CO₂ emissions than GFRPs; meanwhile, thermoplastic resins were observed to have higher carbon emissions than thermoset resins. Song et al. [33] summarized the energy intensities (with unit of MJ/kg) of seven types of resins and four types of fibers. In general, thermoset resins need less energies in their productions as compared to thermoplastic resins, by about 20 % to 50 %; and glass fiber requires much less energy input than carbon fiber.

Moreover, natural fibers, such as China reed fiber and flax fiber, need

the least amount of energies [34]. Favorable features of natural fibers mainly include the lower CO₂ emissions and the energy and carbon credits of end-of-life incineration; and disadvantageous features may include the necessary fertilizer used for cultivation as well as the shorter service life [33–36]. Those pros and cons of natural fibers are to be balanced under the specific circumstances where the FRPs are to be implemented. For FRPs used in civil engineering, a relatively longer service life is typically required (e.g., 20 to 50 years), and thus, glass and carbon fibers are currently preferred over natural fibers. In this regard,

Table 3
Mechanical properties of materials.

Material	Tensile strength (MPa)	Compressive strength (MPa)	Elastic modulus (MPa)	Density (kg/m ³)
Pultruded GFRP structural profile	$f_{Lt} = 768$	$f_{Lc} = 229$	$E_{Lt} = 49160$	$\rho_f = 1900$
FRP rebar	$f_y = 343$	-	$E_f = 70,000$	$\rho_f = 1900$
CFRP rebar	$f_y = 800$	-	$E_f = 210,000$	$\rho_f = 1800$
CFRP sheet	$f_{td} = 1948$	-	$E_f = 210,000$ $E_{fc} \approx 138.4$ for 5 layers	$\rho_f = 1800$
	High modulus	-	$E_f = 435,000$ $E_{fc} \approx 194.9$ for 5 layers	$\rho_f = 1800$
Concrete	C30 $f_{tk} = 2.01$ $f_t = 1.43$	$f_c = 14.3$	$E_c = 30,000$	$\rho_c = 2,500$
	C35 $f_{tk} = 2.20$ $f_t = 1.57$	$f_c = 16.7$	$E_c = 31,500$	$\rho_c = 2,500$
	C40 $f_{tk} = 2.39$ $f_t = 1.71$	$f_c = 19.1$	$E_c = 32,500$	$\rho_c = 2,500$
	C40 (bridge) $f_{tk} = 2.40$ $f_{td} = 1.65$	$f_{cd} = 18.4$	$E_c = 32,500$	$\rho_c = 2,500$
	C50 $f_{tk} = 2.65$ $f_{td} = 1.83$	$f_{cd} = 22.4$	$E_c = 34,500$	$\rho_c = 2,500$
Structural steel	Q235 $f_{sp} = 215$	-	$E_{sp} = 206,000$	$\rho_{sp} = 7850$
	Q355 $f_d = 270$	$f_s = 270$	$E_s = 206,000$	$\rho_s = 7850$
	Q690 $f_s = 690$	-	$E_{sp} = 201,000$	$\rho_{sp} = 7850$
Steel rebar	HRB400 $f_y = 360$	$f_y = 360$	$E_s = 200,000$	$\rho_s = 7850$
	HRB400 (bridge) $f_{sd} = 330$	$f_{sd} = 330$	$E_s = 200,000$	$\rho_s = 7850$
Steel prestressing strand	$f_{pd} = 1260$	$f_{pd} = 390$	$E_s = 195,000$	$\rho_s = 7850$

Where the density of FRP composites is adopted from a design code [45]; each ply of CFRP sheets is 0.167 mm thick; the tensile and compressive strength are the design values, except that f_{tk} is standard value, while the elastic modulus and density are those recommended values by design codes [47,58,59]; E_{fc} is the elastic modulus of multi-layer CFRP sheets, which is calculated with referring to [60]; and C40 (bridge) and HRB400 (bridge) means that those materials are only used in bridges, and they are determined per corresponding design code [47].

this work only focuses on the glass and carbon fiber reinforced composites, namely GFRPs and CFRPs.

2.3. Manufacturing technologies of FRP composites

Aforementioned applications revealed the differences in CO₂ emissions of FRP composites manufactured by different technologies [23–32], including hand layup, vacuum assisted resin transfer molding (VARTM), autoclave molding, compression molding, filament-winding, pultrusion, etc. In particular, pultrusion is a highly automated manufacturing process and commonly known to have the highest cost-efficiency [37]. Thus, pultrusion is seen to have a relatively lower energy requirement [33]. A high extent of automation in manufacturing process could enable a relatively lower energy input and consequently, reduced CO₂ emissions [38]. A similar case is also seen in filament-winding process.

On contrary, hand layup and VARTM have relatively lower extent of automation and thus, are found to exhibit higher CO₂ emissions. Additionally, it was found that the CO₂ emissions of resin transfer molded boat was lower than that made by hand layup. This was attributed to the higher fiber volume ratio realized in resin transfer molding [39]. Indeed, glass fiber has lower embodied CO₂ emissions than polyester resin, by about 65 %, and thus, a higher fiber volume ratio could permit lower

CO₂ emissions [39]. With that being said, it can be rationally inferred that pultruded and filament-wound structural profiles having higher fiber volume ratios are to exhibit lower CO₂ emissions than their counterparts made by hand layup and VARTM processes, when calculated based on unit weight of material.

Despite of having different environmental impacts, selections between those manufacturing technologies are mainly driven by specific applications. For instance, hand layup CFRP sheets are commonly used for strengthening existing structures, and pultruded GFRP structural profiles are dominantly used for constructing new structures such as pedestrian bridges. Different types of FRPs are often not interchangeable considering their pre-designated functionalities. Thus, evaluations of CO₂ emissions of FRP structures/elements must be conducted considering their specific applications.

2.4. Embodied carbon emissions of structural materials

Calculations of carbon emissions of FRP composite structures are carried out based on embodied carbon emissions of materials, which are often given in form of equivalent CO₂ emissions per unit weight of material, denoted as kg CO₂ eq./kg. The embodied CO₂ emissions in manufacturing of FRP composites, steel, and concrete are summarized in Table 1. It is noted that those data are mainly adopted from existing database, among which the most commonly recognized may include inventory of carbon and energy (denoted as ICE) and its updates [40, 41], Composites: Calculating their Embodied Energy (denoted as CEE) [42], and those available from commercial programs such as SimaPro [43]. In addition, a Chinese national standard [44] for calculating carbon emissions of civil infrastructures is adopted in this work, as shown in Table 2. As it can be seen in Tables 1 and 2, there is a relatively large dispersion in existing data. As discussed above, different material compositions and manufacturing technologies could be the reason to the dispersion. In this regard, these data shall be used with special attentions with regard to the practical applications of FRP composites.

3. Structural designs

In civil engineering, the most commonly used FRP composites may be categorized based on their geometries: FRP structural profiles, FRP rebars, and FRP sheets, as shown in Fig. 1. In this work, three major applications of FRPs are analyzed in terms of their carbon emissions, including pultruded FRP pedestrian bridges, FRP rebar-reinforced concrete structures, and FRP sheet-strengthened existing structures. Detailed designs are presented in this section, and the carbon emission are evaluated in next section.

3.1. FRP pedestrian bridges

In this section, pedestrian bridge superstructures spanning from 10 to 30 m were designed using three types of materials, including GFRP structural profiles, structural steel, and reinforced concrete (RC). Multiple design requirements were considered: 1) buckling strength; 2) flexural and shear strength, 3) deflection, 4) crack width, and 5) natural frequency of vibration. The stability and strength limit states are often the first design criteria that must be satisfied, while they are rarely the control ones in practice. Due to the unique material properties, GFRP and steel bridges are often controlled by deflection ($L/250$, in this case) and natural frequency (minimum of 3 Hz, in this case), while RC bridges are typically controlled by crack width. In this work, all types of bridges were designed to meet their requirements by corresponding design codes (e.g., [45–48]). It is noted that only the bridge superstructure was focused in this work; that is, only the main girders were designed. The bridge deck width was set to 5 m in all cases; design dead loads (denotes as DL) included the self-weight of superstructure and 1 kN/m² of pavement; design live load (denotes as LL) was taken as 3.5 kN/m², as prescribed by a design code [49]; and the load combination of

Table 4
Design results of GFRP bridges.

Control limit state	Clear span (m)	Beam height (mm)	Single beam width (mm)	Flange thickness (mm)	Web thickness (mm)	Number of I-beam	Design capacity (kNm)	Actual capacity (kNm)	Deflection (mm)	Deflection limit (mm)	Frequency (Hz)	Material weight (t)
Deflection control	10	300	200	8	6	25	446	698	39	40	10.29	2.28
	12	360	200	10	6	25	655	831	47	48	8.54	3.42
	14	420	200	10	8	25	912	2503	55	56	6.88	4.91
	16	480	200	12	8	25	1221	2823	63	64	5.96	6.79
	18	530	250	14	12	20	1588	5852	70	72	5.20	9.12
	20	610	250	14	12	20	1988	7027	78	80	4.75	11.00
	22	650	500	20	18	10	2434	9364	88	88	4.53	12.90
	24	710	500	22	20	10	2976	11415	95	96	4.10	16.15
	26	770	500	24	22	10	3590	13698	102	104	3.74	19.85
	28	830	500	26	22	10	4237	15976	111	112	3.48	23.01
30	900	500	26	24	10	4967	17989	120	120	3.22	26.82	
Frequency control	10	100	100	8	6	50	438	483	362	40	3.48	1.84
	12	150	100	10	8	50	655	984	254	48	3.40	3.42
	14	210	100	10	8	50	909	1532	220	56	3.36	4.80
	16	250	200	14	12	25	1205	2329	216	64	3.27	6.17
	18	330	250	14	12	20	1532	3210	194	72	3.42	7.17
	20	420	250	14	12	20	1923	4347	174	80	3.44	8.94
	22	500	250	14	12	20	2360	5429	173	88	3.31	10.79
	24	550	250	14	12	20	2833	6140	198	96	3.02	12.42
	26	700	500	18	16	10	3352	5033	153	104	3.48	14.11
	28	800	500	18	16	10	3931	5934	153	112	3.38	16.17
30	850	500	20	16	10	4584	6238	166	120	3.15	18.80	

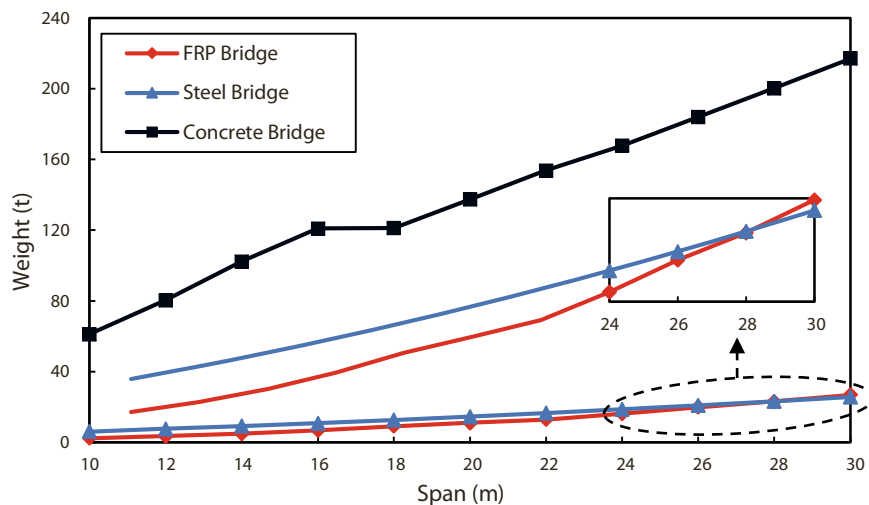


Fig. 3. Weight of materials in pedestrian bridges.

1.3DL+ 1.5LL was used.

First, a total of 11 GFRP bridges were designed in the form of I-beam assemblies, which was adopted from a pedestrian bridge in Beijing, China, as shown in Fig. 2. This section type was selected owing to the high adaptability to various construction environments and the ease of design and installation for FRP practitioners. Detailed design methods are presented in Appendix A.1. Mechanical properties of pultruded GFRP composite are those values previously measured by the present authors [20], as shown in Table 3. Note that the pultruded GFRP composites adopted in this work are manufactured by curved-pultrusion process, through which a camber can be introduced to the beam to ensure the clearance [50]. In the design process, strength and stability limit states were first checked. The strength reduction factors accounting for environmental condition and temperature effect were used in accordance with T/CECS-692 [45], and then, flexural and shear limit states were satisfied accordingly. Moreover, pultruded GFRP profiles are known to have serious buckling issues before reaching their strength limit states [51–56]; in this regard, the widely-accepted Kollár’s

equations [57] were used to calculate the buckling strength.

For FRP bridges, the deflection and natural frequency limit states were focused. The design results are shown in Table 4. It is seen that GFRP bridges are ultimately controlled by deflection limit state. The weight of GFRP materials is plotted against bridge span, as shown in Fig. 3.

Second, 11 steel bridges were designed to have the same deck width, span length, and design loads with GFRP bridges. Detailed design methods are presented in Appendix A.2. All steel bridges were made to consist of two I-shaped girders of which the height was modified along with the span length, as shown in Fig. 4. This section type is often preferred to achieve high economic performance, complete factory fabrication and rapid on-site installation. Necessary flange and web stiffeners were also design, as shown in Fig. 4(a). Structural steel Q355 (see Table 3) was used in all steel bridges. Based on the specified design codes [46,48], the main limit states for steel bridges are the stress level of material, mid-span deflection, and natural frequency. In particular, natural frequency was found to ultimately control the design. The

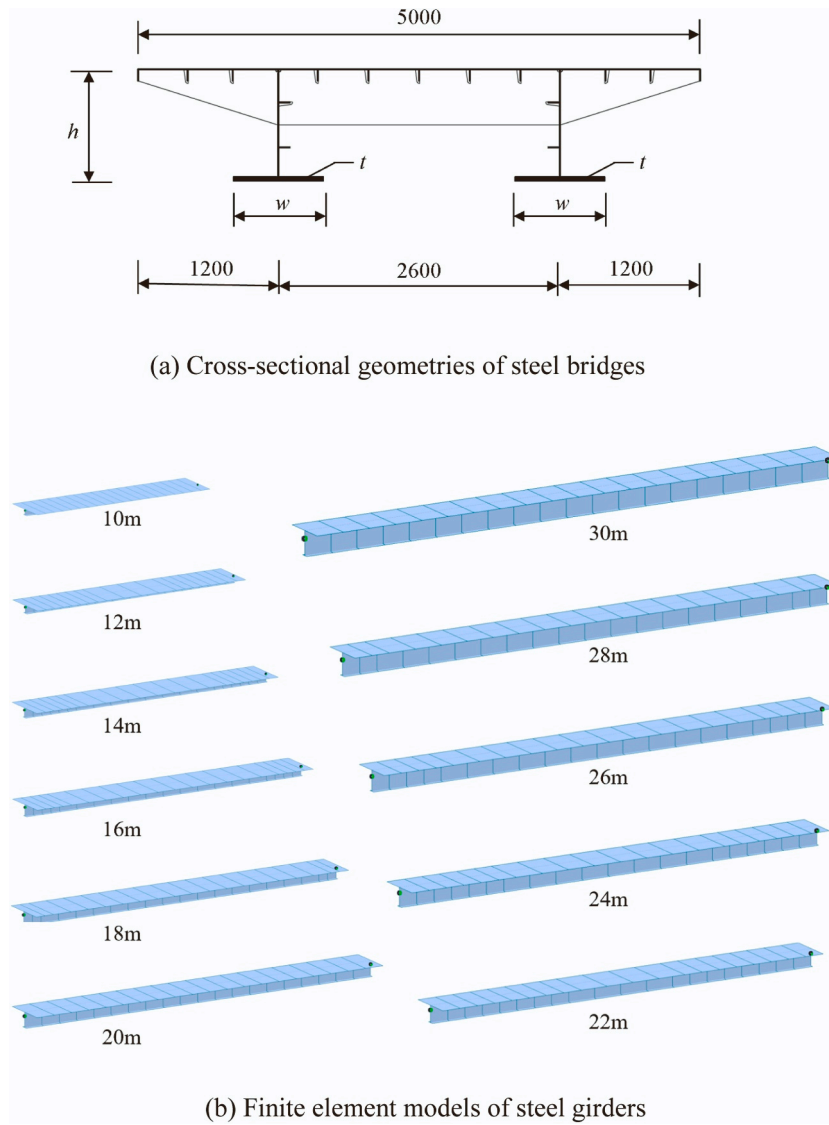


Fig. 4. Schematic of steel bridges (a) Girder spacing was set to 2600 mm, and a 1200 mm cantilever was designed on each side. The deck and web thickness were 10 mm, and stiffeners were designed, as needed. (b) Finite element models of steel girders were constructed for each span length.

Table 5
Design results of steel bridges.

Span length (m)	Beam height (mm)	Bottom flange width (mm)	Bottom flange thickness (mm)	Material weight (t)
10	300	320	14	6.07
12	400	330	14	7.55
14	500	300	16	9.11
16	600	320	16	10.81
18	700	340	16	12.61
20	800	360	16	14.51
22	900	380	16	16.51
24	1000	360	18	18.63
26	1100	380	18	20.85
28	1200	400	18	23.17
30	1300	420	18	25.59

obtained girder height (h), bottom flange width (w) and thickness (t), and the material weight are shown in Table 5.

Third, 11 concrete bridges having the same deck width, span length, and design loads with GFRP and steel bridges were designed. Detailed design methods are presented in Appendix A.3. According to design code

[47], three types of sections were designed for bridges having increasing span length, including reinforced concrete (RC) hollow slab, RC box girder, and prestressed box girder, as shown in Fig. 5. Those section configurations are able to reflect the practical concrete bridges in real scenarios. The main limit states for RC hollow slab girders and RC box girders are flexural and shear strength, and crack width, with the latter being the control one. As for prestressed concrete box girders, it is allowed to have limited tensile stress at bottom of girder while no crack is permitted; thus, the main limit states considered included tensile and compressive stress, and flexural and shear capacities, with the first one being the control limit state. The obtained designs of concrete bridges are shown in Table 6.

3.2. FRP rebar-reinforced concrete structures

In this section, FRP and steel rebars were designed in form of longitudinal and shear reinforcements in concrete beams so as to provide a comparison between their structural performances. A total of 15 simply-supported reinforced concrete (RC) T-beams spanning from 3 to 10 m were designed per design code [58]. The beam span length, spacing and geometries, design dead and live loads, and constituent materials (i.e., concrete and steel) are presented in Table 7. The beam geometries were

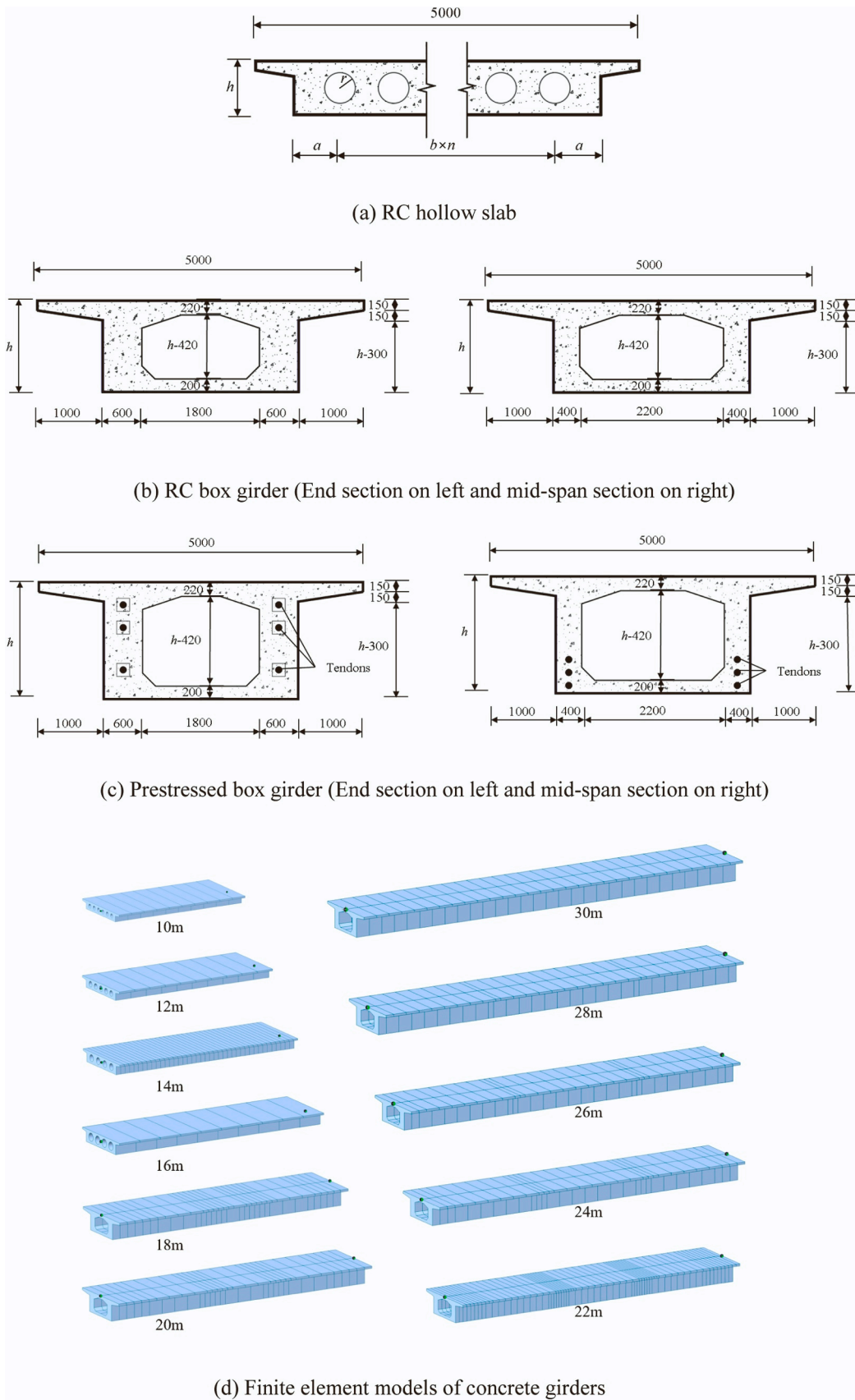


Fig. 5. Section configuration of concrete bridges (a) The hollow slab girder was designed for bridges spanning from 10 to 16 m. (b) The box girder was designed for bridges from 18 to 22 m. (c) The prestressed box girder was designed for bridges from 24 to 30 m. (d) Finite element models of concrete girders were constructed for each span length.

Table 6
Design results of concrete bridges.

Span length (m)	h (mm)	a (mm)	b (mm)	n	r (mm)	Number of steel strands	Flexural rebars	Shear rebars	C40 (t)	C50 (t)	Prestressing strands (t)	HRB400 (t)
10	600	500	600	5	150	-	27 Φ 28	14 Φ 10	55.52	-	-	5.60
12	700	600	700	4	200	-	27 Φ 32	12 Φ 10	73.09	-	-	7.26
14	800	650	900	3	250	-	27 Φ 25 + 27 Φ 25	10 Φ 12	94.04	-	-	8.15
16	900	650	900	3	300	-	27 Φ 28 + 27 Φ 25	10 Φ 12	110.82	-	-	10.02
18	1400	-	-	-	-	-	30 Φ 22 + 30 Φ 20	8 Φ 12	110.62	-	-	10.56
20	1450	-	-	-	-	-	30 Φ 25 + 30 Φ 20	8 Φ 14	124.06	-	-	13.31
22	1500	-	-	-	-	-	30 Φ 25 + 30 Φ 25	8 Φ 14	137.86	-	-	15.74
24	1500	-	-	-	-	$2 \times (9 + 7 + 7)$	6 Φ 18 + 14 Φ 16	8 Φ 14	-	154.58	1.34	11.80
26	1550	-	-	-	-	$2 \times (9 + 9 + 9)$	6 Φ 18 + 14 Φ 16	8 Φ 14	-	169.24	1.69	12.95
28	1600	-	-	-	-	$2 \times (12 + 9 + 9)$	6 Φ 20 + 14 Φ 16	8 Φ 14	-	184.15	2.01	14.09
30	1650	-	-	-	-	$2 \times (12 + 12 + 9)$	6 Φ 20 + 14 Φ 16	8 Φ 14	-	199.48	2.35	15.15

Table 7
Design details of RC beams.

L (mm)	S (mm)	h (mm)	b (mm)	b_f (mm)	h_f (mm)	Concrete-Steel rebar	DL-LL (kN/m ²)	A_s (layout) (mm ²)	M_u (kNm)	RF_M	A_{sv} (mm ²)	V_u (kN)	RF_V
3000	1500	300	120	140	80	C30-HRB400	4.5-3.5	226 (2 Φ 12)	20	1.17	57 (Φ 6 @ 300)	49	3.02
3500	1750	350	140	280	80	C30-HRB400	4.5-3.5	308 (2 Φ 14)	33	1.22	57 (Φ 6 @ 300)	64	2.90
4000	2000	400	160	320	80	C30-HRB400	4.5-3.5	402 (2 Φ 16)	50	1.26	57 (Φ 6 @ 300)	82	2.79
4500	2250	450	180	360	80	C30-HRB400	4.5-3.5	509 (2 Φ 18)	72	1.29	57 (Φ 6 @ 300)	102	2.71
5000	2500	500	200	400	80	C30-HRB400	4.5-3.5	603 (3 Φ 16)	96	1.22	57 (Φ 6 @ 300)	123	2.64
5500	2750	500	200	400	80	C35-HRB400	4.5-3.5	804 (4 Φ 16)	127	1.21	57 (Φ 6 @ 300)	132	2.22
6000	3000	550	220	440	80	C35-HRB400	4.5-3.5	965 (3 Φ 18 + 1 Φ 16)	169	1.27	57 (Φ 6 @ 300)	158	2.23
6500	3250	550	220	440	80	C35-HRB400	4.5-3.5	1251 (1 Φ 25 + 2 Φ 22)	216	1.28	57 (Φ 6 @ 300)	158	1.73
7000	3500	600	240	480	100	C35-HRB400	5.0-3.5	1473 (3 Φ 25)	279	1.24	57 (Φ 6 @ 300)	186	1.65
7500	3750	600	240	480	100	C35-HRB400	5.0-3.5	1853 (3 Φ 25 + 1 Φ 22)	346	1.26	57 (Φ 6 @ 250)	193	1.38
8000	4000	650	260	520	100	C40-HRB400	5.0-3.5	1964 (4 Φ 25)	406	1.18	57 (Φ 6 @ 300)	231	1.51
8500	4250	650	260	520	100	C40-HRB400	5.0-3.5	2413 (3 Φ 32)	492	1.20	57 (Φ 6 @ 200)	252	1.42
9000	4500	700	280	560	100	C40-HRB400	5.0-3.5	2652 (3 Φ 28 + 1 Φ 32)	587	1.22	57 (Φ 6 @ 220)	282	1.42
9500	4750	700	280	560	120	C40-HRB400	5.5-3.5	3445 (2 Φ 25 + 4 Φ 28)	722	1.20	101 (Φ 8 @ 200)	330	1.43
10000	5000	750	300	600	120	C40-HRB400	5.5-3.5	3695 (6 Φ 28)	841	1.20	101 (Φ 8 @ 220)	361	1.39



Where L is clear span length; S is beam spacing; h is overall beam depth; b is web width; b_f is top flange width; h_f is top flange thickness; DL and LL are dead load and live load; A_s is cross-sectional area of longitudinal reinforcement; A_{sv} is cross-sectional area of shear stirrup; M_u is flexural capacity; V_u is shear capacity; and RF_M and RF_V are flexural and shear performance rating factors, respectively.

empirically determined per those recommendations from a design guide [61], and they are believed to represent the real RC beams in practice. In addition, three types of concrete were used for beams having increasing spans, including C30, C35, and C40 (denoted in Chinese conventions), and their mechanical properties are presented in Table 3. Longitudinal reinforcements (for flexure) and stirrups (for shear) are all HRB400 steel (denoted in Chinese convention) which have a yield strength of

360 MPa, as shown in Table 3. Design dead and live loads were determined according to a design standard [62]. Respective load factors for dead and live loads were 1.3 and 1.5; that is, load combination of 1.3DL + 1.5LL was adopted for all cases.

To evaluate the strengthening efficiencies, structural performance rating factor, denoted as RF , was adopted with reference to the load and resistance factor rating method [63]. Value of RF was calculated by Eq.1.

Table 8
Design results of FRP rebars (equivalent strength).

Span <i>L</i> (m)	Steel rebars			GFRP rebars			CFRP rebars		
	<i>A_s</i> (mm ²)	<i>M_u</i> (kNm)	Material weight (kg)	<i>A_f</i> (mm ²)	<i>M_u</i> (kNm)	Material weight (kg)	<i>A_f</i> (mm ²)	<i>M_u</i> (kNm)	Material weight (kg)
3.0	226 (2Φ12)	20	5.33	267 (1Φ12+1Φ14)	21	1.52	101 (2Φ8)	20	0.54
3.5	308 (2Φ14)	33	8.46	355 (1Φ14+1Φ16)	33	2.36	141 (1Φ6+1Φ12)	34	0.89
4.0	402 (2Φ16)	50	12.63	456 (1Φ16+1Φ18)	50	3.46	182 (1Φ6+1Φ14)	51	1.31
4.5	509 (2Φ18)	72	17.98	569 (1Φ18+1Φ20)	71	4.86	226 (2Φ12)	72	1.83
5.0	603 (3Φ16)	96	23.68	694 (1Φ20+1Φ22)	97	6.60	267 (1Φ12+1Φ14)	95	2.40
5.5	804 (4Φ16)	127	34.72	930 (1Φ20+1Φ28)	128	9.72	355 (1Φ14+1Φ16)	127	3.51
6.0	965 (3Φ18+1Φ16)	169	45.43	1107 (1Φ25+1Φ28)	169	12.62	427 (1Φ12+1Φ20)	169	4.61
6.5	1251 (1Φ25+2Φ22)	216	63.84	1473 (3Φ25)	217	18.19	534 (1Φ14+1Φ22)	212	6.25
7.0	1473 (3Φ25)	279	80.92	1742 (2Φ22+2Φ25)	282	23.17	635 (1Φ18+1Φ22)	276	8.00
7.5	1853 (3Φ25+1Φ22)	346	109.08	2213 (2Φ25+2Φ28)	343	31.54	805 (1Φ20+1Φ25)	350	10.87
8.0	1964 (4Φ25)	406	123.31	2338 (1Φ25+3Φ28)	413	35.54	871 (1Φ22+1Φ25)	413	12.54
8.5	2413 (3Φ32)	492	160.99	2904 (1Φ25+3Φ32)	493	46.89	1074 (1Φ20+2Φ22)	509	16.44
9.0	2652 (3Φ28+1Φ32)	587	187.33	3217 (4Φ32)	597	55.01	1140 (3Φ22)	585	18.47
9.5	3445 (2Φ25+4Φ28)	722	256.89	965 (2Φ28+4Φ32)	736	80.30	1473 (3Φ25)	732	25.18
10.0	3695 (6Φ28)	841	290.02	965 (6Φ32)	876	91.68	1597 (2Φ25+1Φ28)	857	28.75

Table 9
Design results of FRP rebars (equivalent stiffness).

Span <i>L</i> (m)	Steel rebars			GFRP rebars				CFRP rebars			
	<i>w_{max}</i> (mm)	Δ_{max} (mm)	Material weight (kg)	<i>A_f</i> (mm ²)	<i>w_{max}</i> (mm)	Δ_{max} (mm)	Material weight (kg)	<i>A_f</i> (mm ²)	<i>w_{max}</i> (mm)	Δ_{max} (mm)	Material weight (kg)
3.0	0.16	6.34	5.33	402 (2Φ16)	0.42	13.95	2.29	129 (1Φ8+1Φ10)	0.40	14.48	0.70
3.5	0.17	7.08	8.46	509 (2Φ18)	0.49	16.69	3.38	163 (1Φ8+1Φ12)	0.48	17.29	1.03
4.0	0.18	7.84	12.63	694 (1Φ20+1Φ22)	0.48	17.75	5.28	226 (2Φ12)	0.46	18.13	1.63
4.5	0.18	8.62	17.98	930 (1Φ20+1Φ28)	0.47	18.51	7.95	308 (2Φ14)	0.44	18.63	2.49
5.0	0.18	9.75	23.68	1232 (2Φ28)	0.44	18.94	11.70	402 (2Φ16)	0.43	19.30	3.62
5.5	0.18	13.51	34.72	1608 (2Φ32)	0.42	24.52	16.81	509 (1Φ16+1Φ18)	0.49	25.70	5.04
6.0	0.18	14.04	45.43	1722 (1Φ25+2Φ28)	0.44	28.41	19.64	628 (2Φ20)	0.48	26.19	6.79
6.5	0.20	18.50	63.84	2463 (4Φ28)	0.32	31.69	30.42	823 (2Φ18+1Φ20)	0.42	31.62	9.63
7.0	0.22	20.34	80.92	2945 (6Φ25)	0.32	34.28	39.17	1008 (2Φ20+1Φ22)	0.45	33.48	12.71
7.5	0.20	25.12	109.08	4199 (2Φ25+4Φ32)	0.24	36.30	59.83	1362 (1Φ22+2Φ25)	0.39	37.14	18.39
8.0	0.21	26.22	123.31	4260 (3Φ28+3Φ32)	0.29	40.26	64.75	1473 (3Φ25)	0.41	39.03	21.21
8.5	0.22	31.41	160.99	5868 (3Φ28+5Φ32)	0.21	42.27	94.78	1963 (4Φ25)	0.32	42.14	30.04
9.0	0.21	31.99	187.33	6245 (1Φ28+7Φ32)	0.24	44.48	106.80	2088 (2Φ25+1Φ28)	0.35	44.36	33.83
9.5	0.19	40.08	256.89	9651 (12Φ32)	0.16	47.37	174.20	3217 (4Φ32)	0.23	47.37	55.01
10.0	0.20	40.89	290.02	9965 (1Φ20+12Φ32)	0.18	49.89	189.34	3445 (2Φ25+4Φ28)	0.25	48.51	62.01

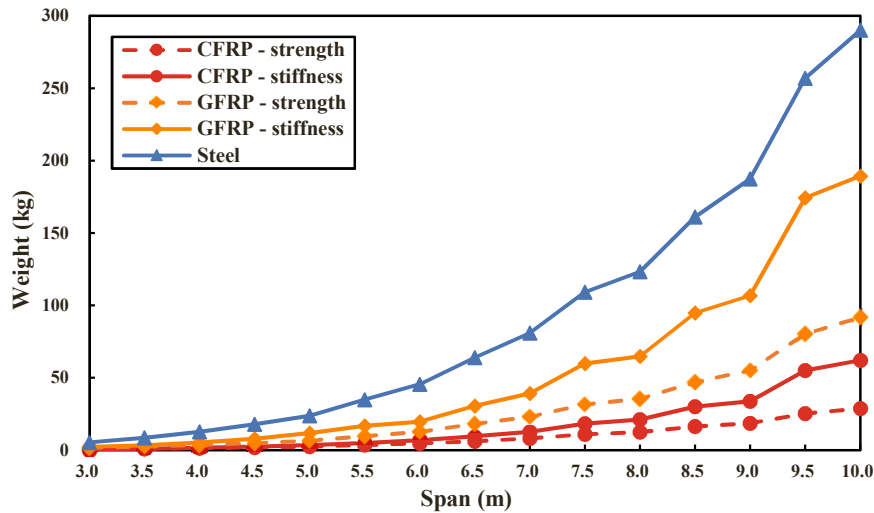


Fig. 6. Weight of rebar in RC beams The weight of steel rebars is higher than that of GFRP and CFRP rebars for all the cases, and this phenomenon becomes more prominent for beams with increasing span length. In addition, designs for equivalent stiffness would require more materials than equivalent strength, and as expected, material weight of GFRP rebar is greater than that of CFRP rebar, due to the relatively lower strength and modulus of glass fiber.

Table 10

Design results of flexural strengthening of RC beams.

Span length L (m)	RF_M (undeteriorated)	RF_M (deteriorated)	CFRP sheet design			Steel plate design		
			Geometries $n \times b \times t$ (mm)	RF_M (strengthened)	Material weight (kg)	Geometries $n \times b \times t$ (mm)	RF_M (strengthened)	Material weight (kg)
3.0	1.17	0.73	1 × 45 × 0.334	1.20	0.08	1 × 70 × 1	1.20	1.65
3.5	1.22	0.77	1 × 60 × 0.334	1.22	0.13	1 × 90 × 1	1.22	2.47
4.0	1.26	0.80	1 × 70 × 0.334	1.20	0.17	1 × 100 × 1	1.18	3.14
4.5	1.29	0.83	1 × 90 × 0.334	1.22	0.24	1 × 65 × 2	1.22	4.59
5.0	1.22	0.77	2 × 50 × 0.334	1.18	0.30	1 × 85 × 2	1.19	6.67
5.5	1.21	0.76	2 × 70 × 0.334	1.21	0.46	1 × 100 × 2.5	1.22	10.79
6.0	1.27	0.81	3 × 50 × 0.334	1.24	0.54	1 × 100 × 2.8	1.24	13.19
6.5	1.28	0.83	3 × 50 × 0.501	1.23	0.88	1 × 100 × 3.4	1.23	17.35
7.0	1.24	0.77	3 × 55 × 0.668	1.21	1.39	1 × 100 × 4.2	1.21	23.08
7.5	1.26	0.79	3 × 70 × 0.668	1.23	1.89	1 × 100 × 5.3	1.23	31.20
8.0	1.18	0.72	3 × 70 × 0.835	1.20	2.53	1 × 100 × 6.5	1.21	40.82
8.5	1.20	0.74	3 × 75 × 1.002	1.20	3.45	1 × 100 × 7.5	1.20	50.04
9.0	1.22	0.75	3 × 70 × 1.503	1.23	5.11	1 × 100 × 8.5	1.23	60.05
9.5	1.20	0.73	3 × 75 × 2.004	1.21	7.71	1 × 100 × 10	1.19	74.58
10.0	1.20	0.73	3 × 80 × 2.004	1.19	8.66	2 × 100 × 5.5	1.19	86.35

n indicates the number of CFRP sheets or steel plates; b indicates the width of CFRP sheets or steel plates; t indicates the thickness of each CFRP sheet or steel plate.

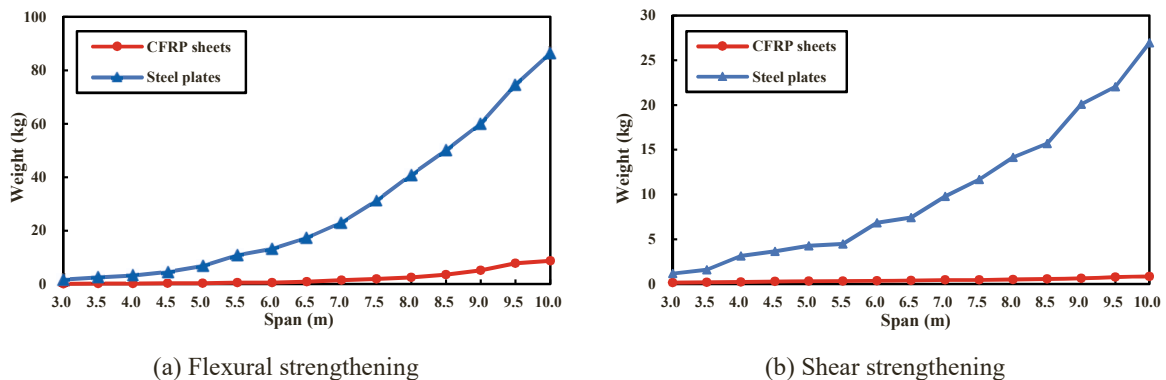


Fig. 7. Weight of materials in strengthening of RC beams.

In this case, RF was kept about 1.20 for the moment capacities of all RC beams (denoted as RF_M) and kept as (at least) 1.40 for the shear performance (denoted as RF_V). With the design of RC beams completed, the

resulting RF_M and RF_V values were obtained, as shown in Table 7.

Table 11

Design results of shear strengthening of RC beams.

Span length L (m)	RF_V (undeteriorated)	RF_V (deteriorated)	CFRP sheet design		Steel plate design	
			RF_V (strengthened)	Material weight (kg)	RF_V (strengthened)	Material weight (kg)
3.0	3.02	2.72	3.74	0.15	3.74	1.17
3.5	2.90	2.63	3.59	0.18	3.58	1.60
4.0	2.79	2.56	3.48	0.22	3.49	3.14
4.5	2.71	2.50	3.39	0.28	3.40	3.64
5.0	2.64	2.45	3.34	0.31	3.34	4.29
5.5	2.22	2.06	2.82	0.33	2.83	4.49
6.0	2.23	2.08	2.84	0.37	2.84	6.83
6.5	1.73	1.61	2.25	0.38	2.24	7.43
7.0	1.65	1.53	2.20	0.45	2.19	9.81
7.5	1.38	1.26	1.89	0.45	1.89	11.68
8.0	1.51	1.42	2.02	0.49	2.03	14.15
8.5	1.42	1.29	1.91	0.57	1.90	15.69
9.0	1.42	1.30	1.92	0.62	1.93	20.08
9.5	1.43	1.23	1.86	0.78	1.86	22.04
10.0	1.39	1.22	1.85	0.84	1.85	26.94

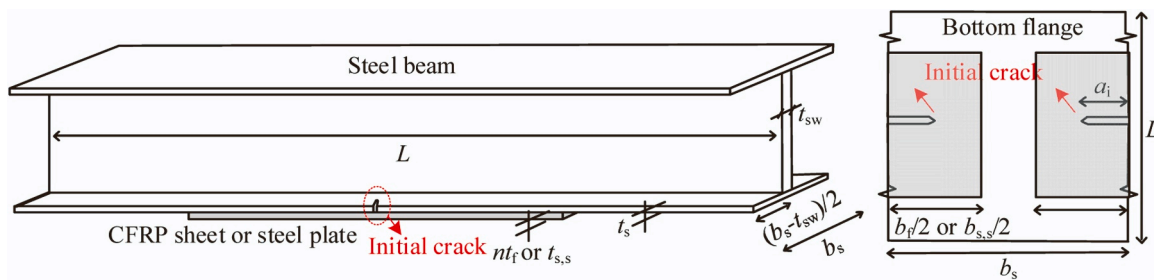


Fig. 8. Schematic of cracked steel beam and its fatigue strengthening nt_f and $t_{s,s}$ are the thickness of CFRP composite and steel plate for strengthening, respectively; n is the layer number; t_f is the thickness of one layer CFRP sheet; b_f and $b_{s,s}$ are the width of CFRP composite and steel plate, respectively; L is the length of steel beam; b_s and t_s are the thickness and width of steel beam flange, respectively; t_{sw} is the thickness of web; and a_i is the initial crack length by one edge.

$$RF = \frac{\text{Load capacity} - \text{Dead loads}}{\text{Live loads}} \quad (1)$$

In this section, steel rebars in RC beams (see Table 7) were replaced by GFRP and CFRP rebars following two strategies: equivalent strength and equivalent stiffness. Detailed design methods are presented in Appendix B. For evaluating the equivalent strength, the flexural capacity M_u of beam was adopted, and for evaluating the equivalent stiffness, the maximum crack width w_{max} and maximum deflection Δ_{max} were adopted. Material properties of GFRP and CFRP rebars are those recommended by design code [59], as shown in Table 3. The obtained designs are shown in Tables 8 and 9, and Fig. 6.

3.3. FRP sheet-strengthened existing structures

3.3.1. Strengthening of concrete beams

In this section, FRP sheet was compared with steel plate in strengthening of concrete beams, and only CFRP sheet was selected considering its dominant application in this field. Those RC beams designed in previous section was adopted, as shown in Table 7. In order to simulate the deteriorated RC beams, appropriate degradations of steel rebars were assumed. The degradation mechanism reported by Imperatore et al. [64] and Vanama and Ramakrishnan [65] was adopted; that is, 20 % loss of weight would lead to 20 % loss of strength, while the modulus basically remained unchanged. It is noted that the concrete was assumed to be intact in terms of both strength and modulus. Then, deteriorated RC beams were found to have RF_M values generally in the range between 0.70 and 0.80.

Two strengthening methods, CFRP sheets and steel plates, were designed in accordance with appropriate design codes [59,66]. Detailed design methods are presented in Appendix C.1. Mechanical properties of

CFRP sheets and steel plates (i.e., structural steel Q235, in Chinese convention) are shown in Table 3. The goal of both strengthening methods was to recover the RF_M back to 1.20. The obtained strengthening methods are presented in Table 10 and Fig. 7(a). It should be noted that CFRP sheets typically fail in the manner of interface debonding, rather than reaching its tensile strength limit state [67], while steel plates are able to reach the yield strength of material. In this work, the actual failure modes of both strengthening methods were respected. Thus, for CFRP sheets, multiple layers of sheets were applied to avoid the interfacial failure. Each sheet was composed of multiple CFRP prepregs (each prepreg having a thickness of 0.167 mm).

In addition to flexural strengthening, shear strengthening was also conducted. The design results are shown in Table 11 and Fig. 7(b). All RC beams only adopted the minimum shear stirrup per requirement, and the resulting RF_V values were all found to be greater than 1.00, especially for those beams having relatively shorter spans (e.g., 3 to 6 m). In this work, those RC beams were assumed to be deteriorated to the extent to which the effect of shear strengthening can be observed. In Table 11, it is seen that all RC beams were shear-strengthened to the same level (i.e., the same RF_V factors) and the weight of CFRP sheets is much less than steel plates.

3.3.2. Strengthening of steel beams

In this section, CFRP sheets were used to enhance the fatigue behavior of cracked steel beam. Detailed design methods are presented in Appendix C.2. The cracks in bottom flange (i.e., two initial cracks at the two edges) were designed to follow those studies in available literature [68-70]. Two strengthening methods (i.e., CFRP sheets and steel plates) were designed according to design codes [59,71]. The strengthening scheme is shown in Fig. 8. The length of strengthening material was taken as 1 m. Three strengthening materials were

Table 12
Design results of fatigue strengthening of steel beams.

b_s (mm)	t_s (mm)	a_i (mm)	N ($\times 10^3$)	Normal modulus CFRP sheet			High modulus CFRP sheet			Steel plate					
				Geometries $n \times b_i \times t_i$ (mm)	N ($\times 10^3$)	RF (strengthened)	Material weight (kg)	Geometries $n \times b_i \times t_i$ (mm)	N ($\times 10^3$)	RF (strengthened)	Material weight (kg)	Geometries $b_s \times t_{s,s}$ (mm)	N ($\times 10^3$)	RF (strengthened)	Material weight (kg)
200	10	5	1541	$5 \times 196 \times 0.167$	1869	1.21	0.31	$5 \times 140 \times 0.167$	1871	1.21	0.22	38×3	1874	1.22	0.89
200	10	6	1390	$5 \times 182 \times 0.167$	1671	1.20	0.29	$5 \times 130 \times 0.167$	1673	1.20	0.21	35×3	1672	1.20	0.82
200	10	7	1267	$5 \times 182 \times 0.167$	1531	1.21	0.29	$5 \times 130 \times 0.167$	1533	1.21	0.21	35×3	1532	1.21	0.82
200	10	8	1165	$5 \times 182 \times 0.167$	1414	1.21	0.29	$5 \times 130 \times 0.167$	1416	1.22	0.21	35×3	1415	1.21	0.82
200	10	9	1077	$5 \times 168 \times 0.167$	1293	1.20	0.27	$5 \times 120 \times 0.167$	1294	1.20	0.19	32×3	1291	1.20	0.75
200	10	10	999	$5 \times 168 \times 0.167$	1205	1.21	0.27	$5 \times 120 \times 0.167$	1206	1.21	0.19	32×3	1204	1.21	0.75

considered. Two types of CFRPs having normal and high moduli were applied. Material properties are shown in Table 3. Alternatively, considering the high stress concentration at cracked region, a high strength steel plate (denoted as Q690 in Chinese convention) was adopted.

The elastic modulus E_s of steel is 201 GPa [72], and the yield point f_s is 690 MPa. A typical loading case was considered; that is, the fatigue stress range of the bottom flange was 100 MPa with a stress ratio of 0.1. As shown in Table 12, six beams were designed with different geometrics and loading conditions.

The fatigue life N of strengthened steel structures was calculated following the method in literature [60,73]. The ratio of fatigue life N after and before strengthening was defined as RF , and in this work, the fatigue life N was designed to be enhanced by 20 % (i.e., $RF=1.20$). The design results are shown in Table 12. The weight of strengthening materials is plotted against the initial crack length a_i , as shown in Fig. 9.

4. Carbon emissions

Carbon emissions of three types of FRP composite structures were analyzed in this section. In particular, pedestrian bridges were analyzed in terms of material manufacturing, transportation, construction and maintenance, while FRP rebar-reinforced concrete structures and FRP sheet-strengthened existing structures were addressed considering material manufacturing.

4.1. Material manufacturing

The carbon emissions produced in material manufacturing were calculated following Eq. 2 [44].

$$C_{pro} = \sum M_i F_i \quad (2)$$

Where C_{pro} is the carbon emission of materials (unit: kg CO₂ eq.); M_i is the weight of i th material (unit: kg); and F_i is the carbon emission factor of i th material (unit: kg CO₂ eq./kg). The weights of materials used in three types of FRP applications were determined in previous sections, including the weights of FRP composites, concrete and/or steel. In addition, carbon emission factors F were adopted from available literature and existing database (see Tables 1 and 2).

Evidently, the value of F is extremely important in calculation of carbon emissions. A relatively large variation is identified in F values of FRP composites. Such discrepancies mainly result from the inherent variations of materials, such as the different fiber type/fraction in FRPs, different manufacturing technologies, etc. In this regard, an appropriate set of F values must be selected based on specific types of materials addressed in this work. For CFRP sheets and CFRP rebars, F value was taken as 10.09, which was adopted from CEE [42] (see Table 2). For GFRP rebars and pultruded GFRP structural profiles, F value was taken as 2.16, which was the average value of the data prescribed by CEE [42], 1.23, and that reported by Tanaka et al. [24], 3.09.

On the other hand, F values of concrete, steel rebar and structural steel were taken as those prescribed by a design code GB/T51366 [44]. Specifically, F value was taken as 0.12 for C30 concrete, 0.135 for C40 concrete, and 0.15 for C50 concrete. For steel rebar, F value was taken as 2.34, and for structural steel, F value was 2.05.

4.1.1. FRP pedestrian bridges

Carbon emissions of three types of pedestrian bridges are presented in Fig. 10. The carbon emission factor of pultruded GFRP structural profiles was taken as 2.16 (i.e., the average of 1.23 [42] and 3.09 [24]). Given the large variation in existing data, both the lower bound and upper bound carbon emissions of GFRP bridges were calculated, as shown by the shaded area in Fig. 10.

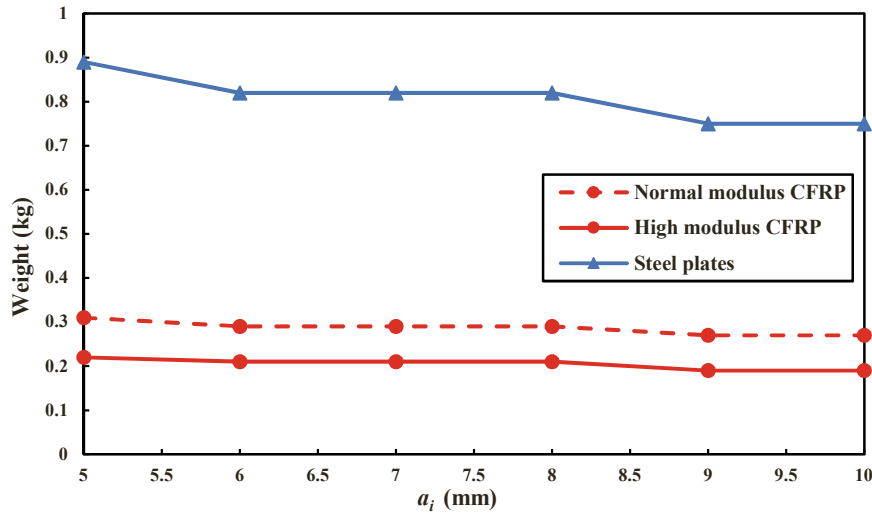


Fig. 9. Weight of materials in strengthening of steel beams High modulus CFRP yields the lowest weight, while steel plate yields the highest weight, nearly four times of the high modulus CFRP.

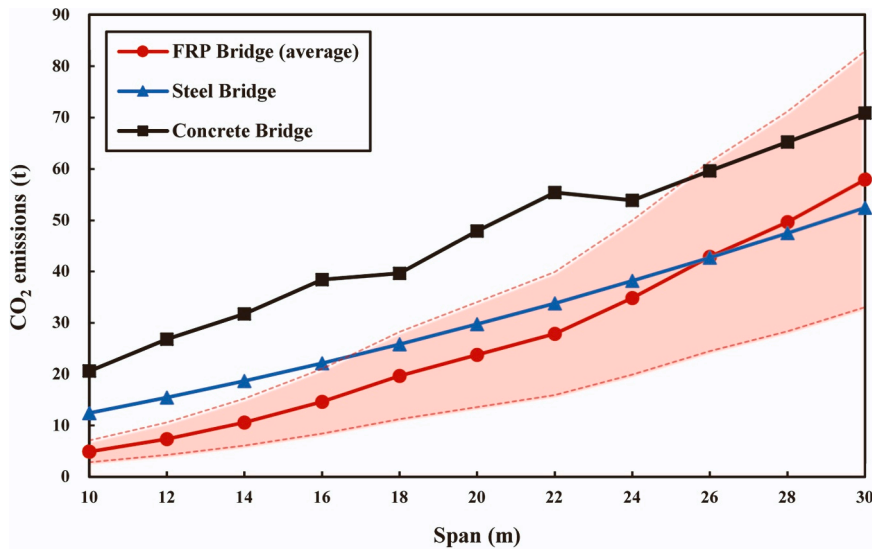


Fig. 10. Carbon emissions of pedestrian bridges (material manufacturing) When taking the average carbon emission factor of pultruded GFRP composite (i.e., $F = 2.16$), for the shortest span of 10 m, carbon emissions produced by GFRP bridge are less than those of steel and concrete bridges by 60 % and 76 %, respectively; for the intermediate span of 20 m, carbon emissions of GFRP bridge are reduced by 20 % and 50 % as compared to steel and concrete bridges, respectively; and for the greatest span of 30 m, GFRP bridge is able to reduce the carbon emissions by 18 % as compared to concrete bridge and to increase the carbon emissions by 10 % as compared to steel bridge. If taking the upper bound carbon emission of GFRP composite, GFRP bridges could still show a better environmental performance for spans from 10 to 16 m, and this span range is often acceptable for pedestrian bridges. As for the lower bound carbon emission of GFRP composite, GFRP bridges have uniformly lower carbon emissions as compared to steel and concrete bridges.

4.1.2. FRP rebar-reinforced concrete structures

The carbon emissions produced in material manufacturing (i.e., FRP rebars and steel rebars) are shown in Fig. 11. Evidently, using CFRP and GFRP rebars to replace steel rebars in concrete structures could permit reduced carbon emissions. For all spans being addressed, using CFRP rebars the average carbon reductions realized by equivalent stiffness and strength with steel rebars are 27 % (standard deviation, STD = 13 %) and 54 % (STD = 1 %), respectively. Then, using GFRP rebars the average carbon reductions realized by equivalent stiffness and strength with steel rebars are 53 % (STD = 8 %) and 73 % (STD = 1 %) for all spans, respectively.

4.1.3. CFRP sheet-strengthened existing structures

For strengthening of concrete beams, carbon emissions produced in

material manufacturing (i.e., CFRP sheets and steel plates) are presented in Fig. 12. It is noted that Fig. 12 accounts for the total carbon emissions of both the materials used in flexural and shear strengthening. CFRP sheets are observed to effectively reduce the carbon emissions as compared to steel plates. It is seen that for all spans being addressed, replacing steel plates by CFRP sheets the average carbon reductions is 72 % (STD = 6 %).

For strengthening of steel beams, carbon emissions produced in material manufacturing (i.e., CFRP sheets and steel plates) are presented in Fig. 13. CFRP sheets are seen not to reduce the carbon emissions in strengthening the fatigue behavior of cracked steel beams.

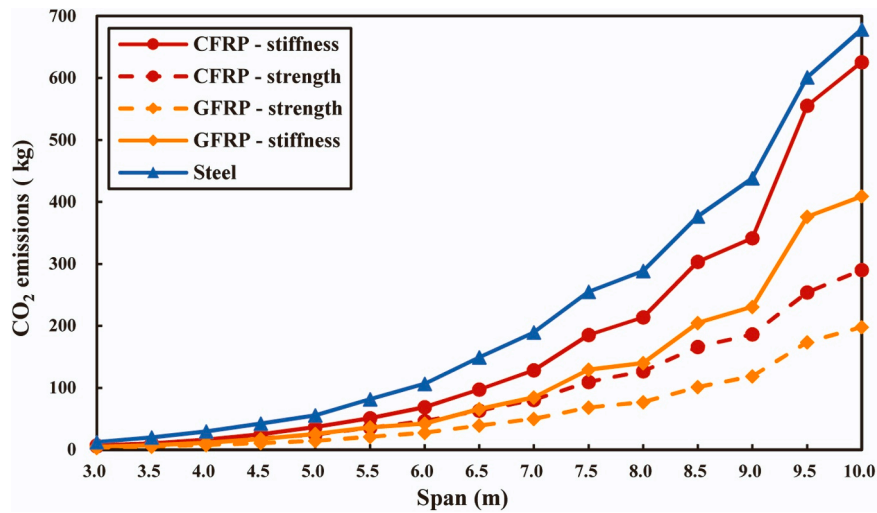


Fig. 11. Carbon emissions of rebar in RC beams (material manufacturing) Both GFRP and CFRP rebar could lead to reduced carbon emissions, and this is valid for both equivalent strength and equivalent stiffness strategies. GFRP rebar showed much lower carbon emissions as compared to CFRP rebar, which is mainly due to higher embodied carbon emissions of carbon fiber.

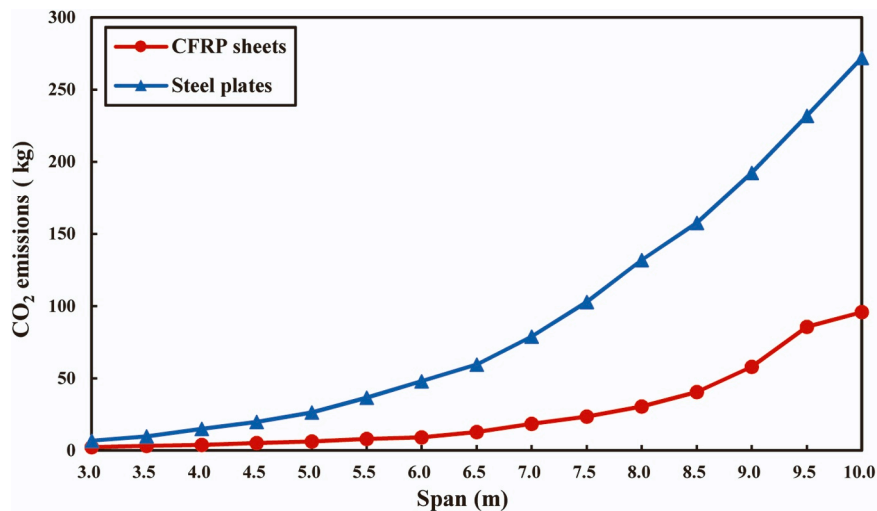


Fig. 12. Carbon emissions of strengthening RC beams (material manufacturing) Given the same strengthening efficiencies, CFRP sheets are observed to produce less CO₂ emissions than steel plates.

4.2. Transportation

The carbon emissions produced in transporting the materials from manufacturing plant to construction site were calculated following the method prescribed by GB/T-51366 [44], as shown in Eq. 3. Only the pedestrian bridge was analyzed at this stage due to the relatively greater amount of materials.

$$C_{trans} = \sum M_i D_i T_i \tag{3}$$

Where C_{trans} is the carbon emissions produced in transportation (unit: kg CO₂ eq.); M_i is the weight of i th material (unit: ton); D_i is the transportation distance of i th material (unit: km); and T_i is the carbon emission factor of the vehicle (unit: kg CO₂ eq./ (ton·km)).

The transportation distance of concrete was taken as 40 km. This distance was determined considering the allowable truck speed in city area and the allowable transporting time of concrete [44]. In addition, the transportation distance for pultruded GFRP structural profiles and structural steel was empirically taken as 100 km, considering FRP and steel plants are often farther away from city center. The carbon emission

factor of a 10-ton diesel truck is 0.162 kg CO₂ eq./ (t·km) [44]. The resulting carbon emissions produced in transportation stage are shown in Fig. 14.

4.3. Construction

The carbon emissions produced in constructions of three types of pedestrian bridges were calculated. Again, FRP sheets and rebar were not discussed, since their construction methods are relatively straightforward and to some extent, similar to their steel counterparts, especially for FRP rebar. In addition, a precise calculation of carbon emissions produced in construction stage would require detailed CO₂ data pertaining to all construction equipment as well as the building workers. To simplify the calculation, construction-related carbon emissions were estimated based on available data from literature, as shown in Table 13.

From Table 13, it is seen that the average carbon emissions occurred in construction stage is about 4.2 % of the total CO₂ emissions for FRP bridge, and that value is 8.0 % for steel bridge and 7.8 % for concrete bridge. Thus, using those empirical factors, carbon emissions in

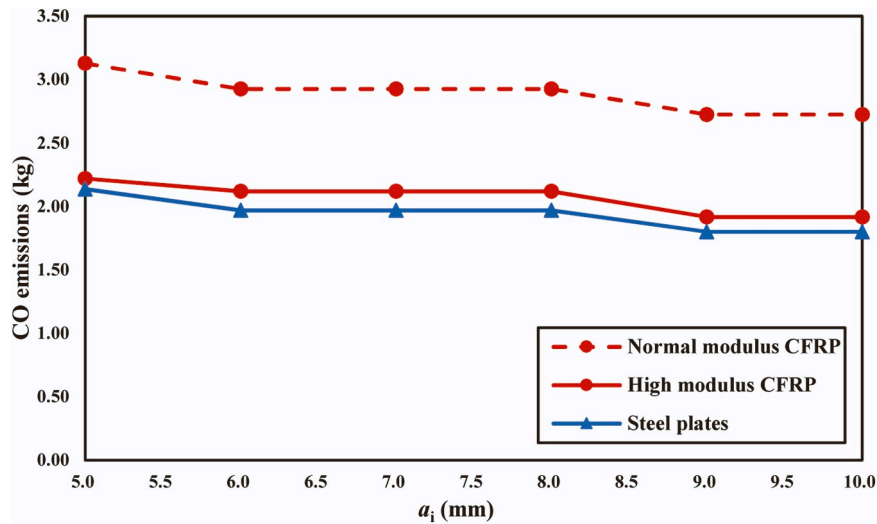


Fig. 13. Carbon emissions of strengthening steel beams (material manufacturing) CFRP sheets with high modulus showed slightly higher CO₂ emissions than steel plates, with difference about 7 %, and the other CFRP sheets with normal modulus exhibited much higher CO₂ emissions, by about 33 %.

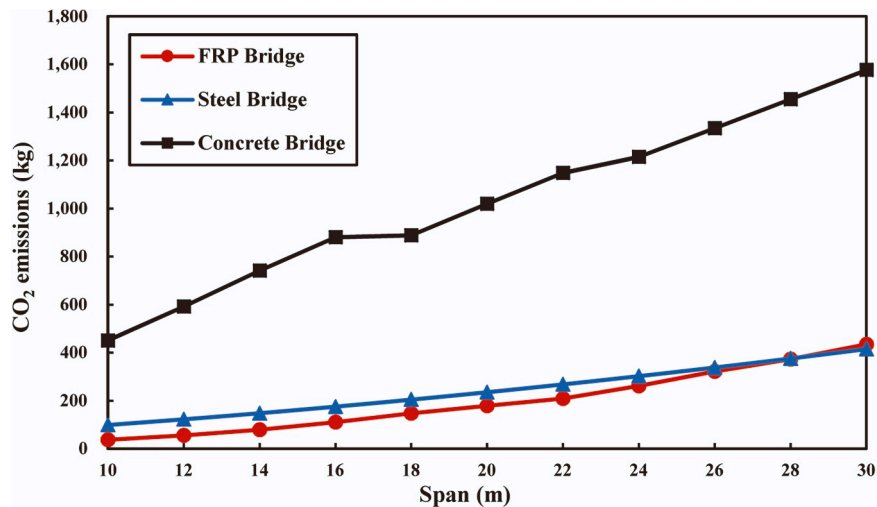


Fig. 14. Carbon emissions of pedestrian bridges (transportation) Concrete bridges, having significantly higher weight of materials, produce the greatest carbon emissions in transportation, although the transportation distance of concrete is 60 % shorter than that of pultruded FRP composites and structural steel. FRP bridges, in general, exhibit the least amount of carbon emissions in transportation, except for the span of 30 m.

Table 13
Life-cycle carbon emissions in literature.

Bridge type	Source	Material manufacturing		Transportation		Construction		Maintenance		Total CO ₂ emissions (ton)
		CO ₂ emissions (t)	CO ₂ fraction	CO ₂ emissions (t)	CO ₂ fraction	CO ₂ emissions (t)	CO ₂ fraction	CO ₂ emissions (t)	CO ₂ fraction	
FRP Bridge	Dai and Ueda[25]	130.0	97.4 %	-	-	3.5	2.6 %	-	-	133.5
	Zhang et al.[43]	5.3	90.1 %	0.0640	1.1 %	0.5	8.2 %	-	-	5.884
	Li et al.[28]	0.3	98.0 %	0.0055	2.0 %	-	-	-	-	0.2755
	Jena and Kaewunruen[74]	160.0	98.2 %	-	-	2.9	1.8 %	-	-	162.292
Steel Bridge	Tan[75]	26249.7	94.9 %	561.1	2.0 %	751.0	2.7 %	100.9	0.4 %	27662.7
	Xu[76]	1902.8	71.9 %	2.3	0.1 %	113.8	4.3 %	629.1	23.8 %	2648.0
	Zhang[77]	2489.2	62.1 %	59.8	1.5 %	403.6	10.1 %	1058.1	26.4 %	4010.7
	Li et al.[28]	6.1	83.6 %	0.1	1.4 %	1.1	15.1 %	-	-	7.3
Concrete Bridge	Tan[75]	1108.9	90.0 %	17.0	1.4 %	83.2	6.8 %	22.4	1.8 %	1231.5
	Xu[76]	2499.9	75.8 %	3.5	0.1 %	165.3	5.0 %	629.1	19.1 %	3297.8
	Zhang[77]	2281.4	58.7 %	64.4	1.7 %	419.0	10.8 %	1124.5	28.9 %	3889.3
	Li et al.[28]	8.6	84.3 %	0.8	7.8 %	0.9	8.8 %	-	-	10.2

Note: CO₂ fraction indicates the ratio of respective CO₂ emissions to total CO₂ emissions.

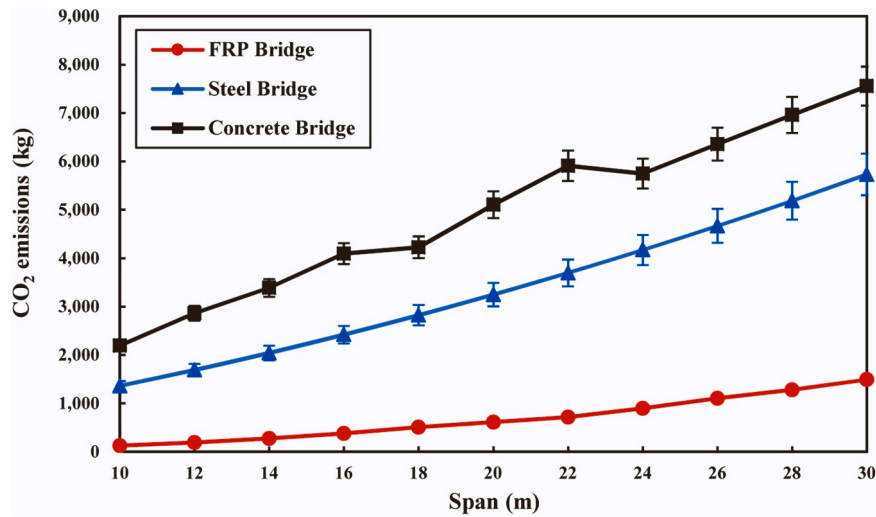


Fig. 15. Carbon emissions of pedestrian bridges (construction).

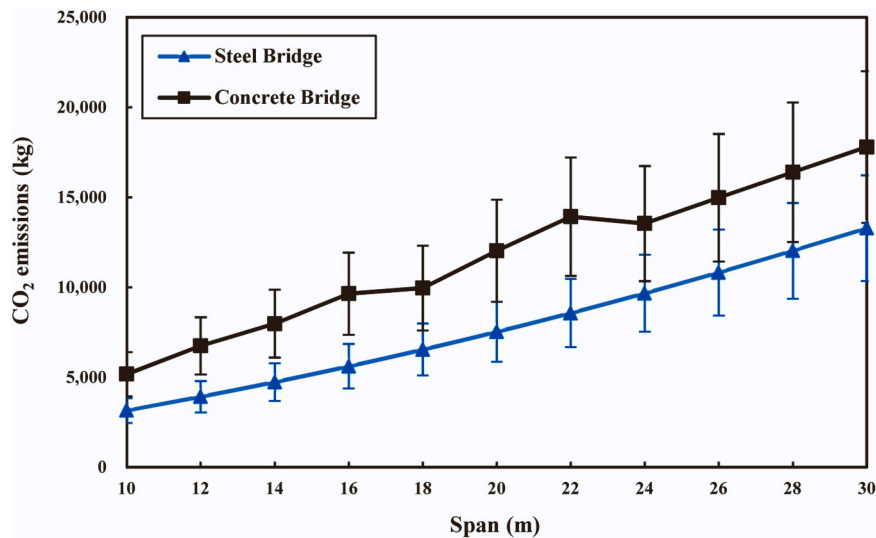


Fig. 16. Carbon emissions of pedestrian bridges (maintenance).

construction stage can be estimated, as shown in Fig. 15. The error bars indicate one standard deviation (STD), and STDs are 4.17 %, 7.48 %, and 5.35 % for FRP, steel, and concrete bridges, respectively. In general, carbon emissions in construction stage follow the same trend as that in material manufacturing stage. FRP bridge, again, shows the least amount of carbon emission as compared to other two types of bridges. For all spans being addressed, the average carbon reductions realized by FRP bridge in construction stage are 82 % (STD = 6 %) and 88 % (STD = 5 %) and as compared to steel and concrete bridges, respectively.

4.4. Maintenance

The carbon emissions produced in maintenance stage of three types of pedestrian bridges were estimated. Again, those data shown in Table 13 was adopted. The average fractions of maintenance-related CO₂ emissions are 16.8 % and 16.6 % for steel and concrete bridges, respectively. For FRP bridge, maintenance was neglected. The estimated carbon emissions in maintenance are shown in Fig. 16. The error bars indicate one standard deviation (STD), and STDs are 22.10 % and 23.64 % for steel and concrete bridges, respectively.

4.5. Carbon emissions of pedestrian bridge

Total carbon emissions of three types of pedestrian bridges were analyzed, as shown in Fig. 17. In addition, specific fractions of CO₂ emissions produced in each stage were calculated, as shown in Fig. 18. For all bridge spans being addressed, the total carbon emissions of FRP bridges are reduced by 66 % (STD = 10 %) and 77 % (STD = 9 %) as compared to steel and concrete bridges, respectively.

5. Discussions

5.1. Direct and indirect carbon reductions

In this work, it is demonstrated that direct carbon reductions can be realized by FRP composite structures in civil engineering, including all-FRP structures (i.e., pedestrian bridges), FRP reinforced-concrete structures, and FRP strengthened-existing structures, as shown in Fig. 19. In addition, to the best knowledge of present authors, two indirect carbon reductions may be achieved through FRP composites. Concrete carbonation is known to be able to absorb CO₂ from atmosphere [78]. However, this chemical process could lead to severe corrosion of steel rebars. With the durable FRP rebars, concrete

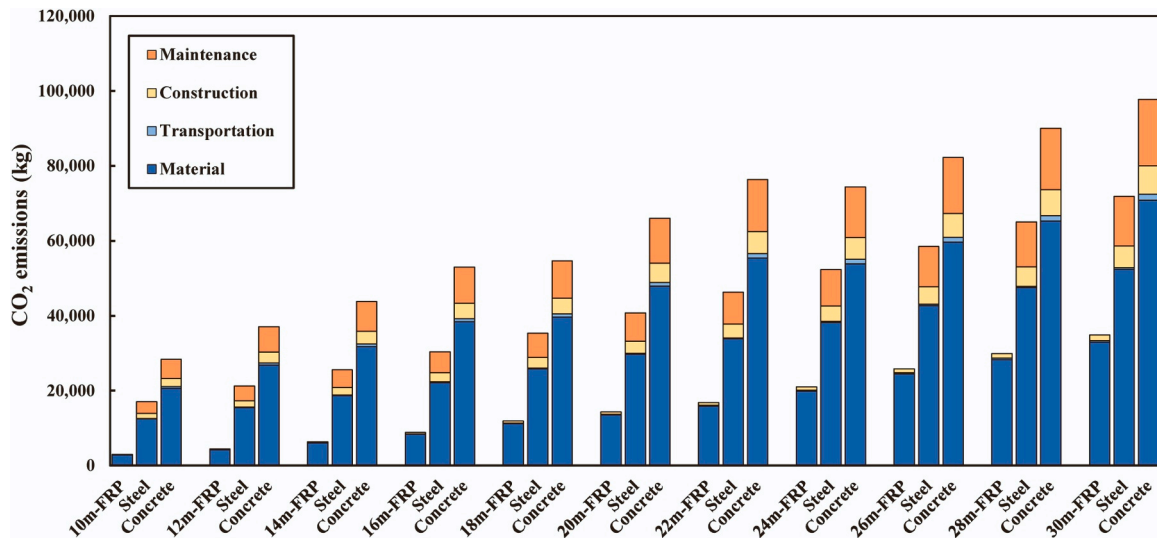


Fig. 17. Life-cycle carbon emissions of pedestrian bridges The overall carbon emissions of concrete bridges are the highest, followed by steel bridges. FRP bridges exhibit the least amount of life-cycle carbon emissions. In particular, when compared to steel and concrete bridges, the total carbon emissions of FRP bridges are reduced by 66 % and 77 % for all spans being addressed, respectively.

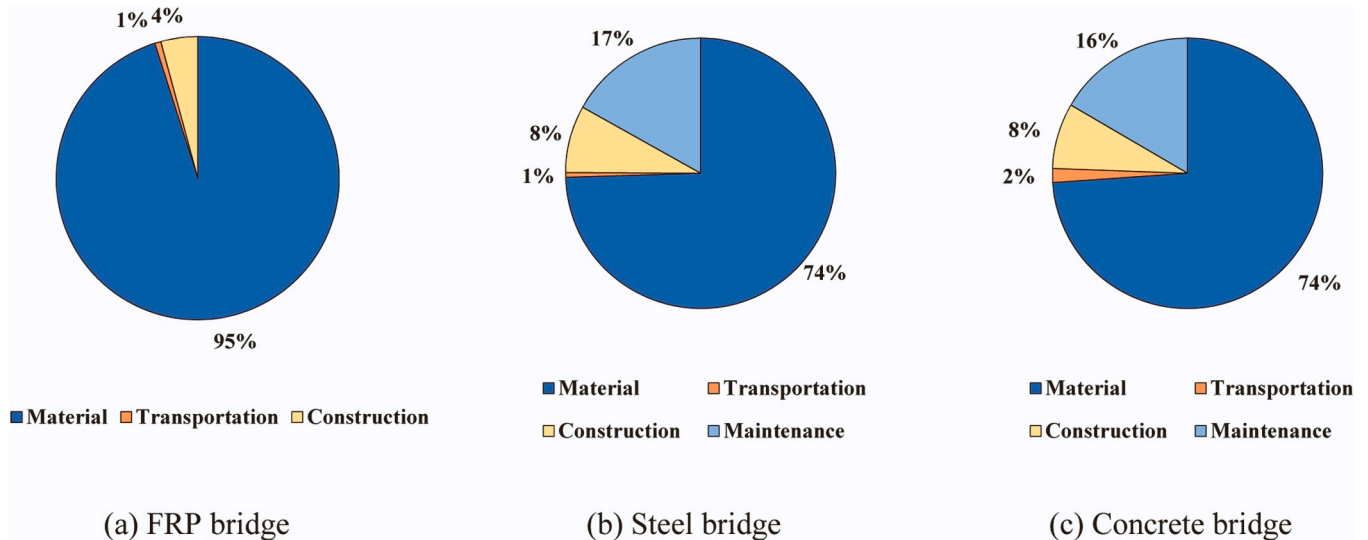


Fig. 18. Emission fractions of pedestrian bridges Material manufacturing takes the dominant fraction of the life-cycle carbon emissions of FRP bridges, by about 95 %, while the construction and transportation only account for 5 % of the total carbon emissions. For steel and concrete bridges, material manufacturing also takes the dominant fraction of their total carbon emissions, though their fractions reduce to 74 %. It is worth noting that maintenance takes the second largest fraction for steel and concrete bridges, which is believed to be able to represent the real scenarios in the field. Moreover, steel and concrete bridges show a higher fraction for construction than FRP bridge; indeed, the lighter weight of FRP bridge could permit a shorter construction time.

carbonation is therefore permitted, thus contributing to reducing the carbon emissions in the long run. Moreover, FRP composites are increasingly used in buildings and houses as thermal enclosures. FRP enclosure has a much lower thermal conductivity as compared to metallic materials and thus, is able to promote the energy conservations as well as carbon reductions [79,80]. It is noted that the indirect carbon reductions are recommended herein as potential benefits of FRP composites from a broad view, and their quantified carbon reductions shall be investigated in the next stage.

5.2. Methodology evaluations

First, in this work the carbon emissions of FRP composite structures are investigated through carbon footprints mainly produced in the stage of material manufacturing. Despite of not having a standard life-cycle

assessment, the observed carbon footprints could effectively provide civil engineers and policy makers a rapid and credible knowledge on the general environmental impact of FRP composites and their structures. In order to acquire a complete knowledge of environmental impact of FRP structures, a standard life-cycle assessment on the carbon emissions shall be conducted following ISO 14040 [81] or those studies reported by Chen et al. [82] and Zhou et al. [83]. The life-cycle carbon emissions of FRP composites may be evaluated in the process shown in Fig. 20.

Second, the carbon emission factors have a decisive impact on evaluating the environmental performance of FRP composite structures. In this work, those factors are adopted from available literature and database. However, a noticeable variation is identified in existing database, and the existing standards have not included any prescriptions on FRP composites. In order to improve the accuracy of this analysis, carbon emission factors are to be first investigated. Those factors should

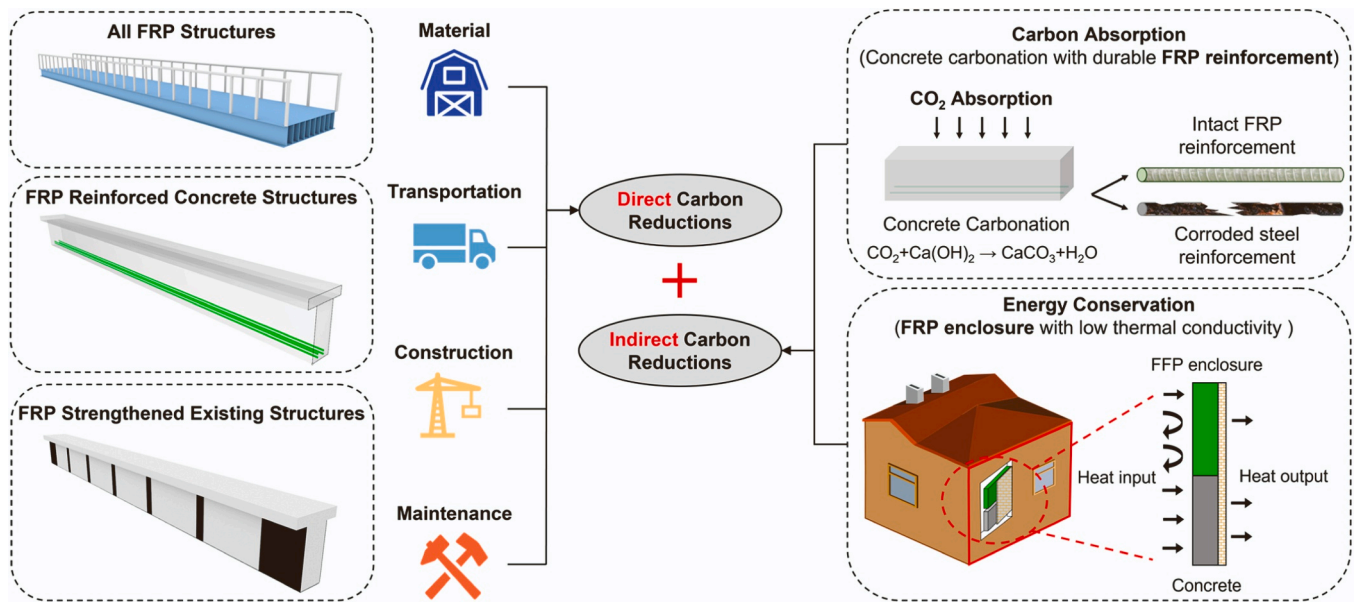


Fig. 19. Carbon reductions realized by FRP composites in civil engineering.

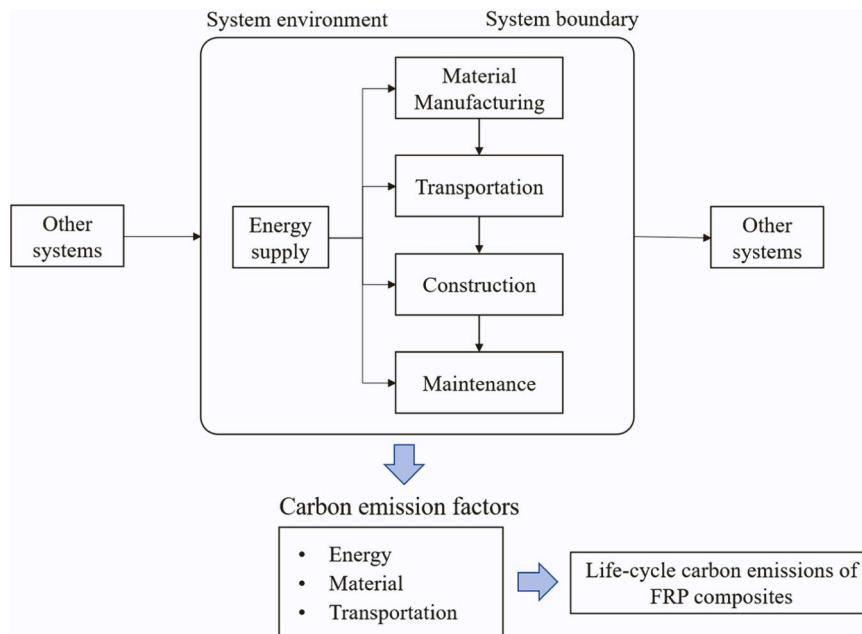


Fig. 20. Method of evaluating life-cycle emissions of FRP composites.

capture the real environment where the FRP structure is to be built. The local power generation, local raw material manufacturing, and local transportation, together, may have a coupled influence on the carbon emission factor of a certain type of construction material. With that being said, carbon emission factors might be rationally different for different countries or regions. In this regard, future work is needed to establish localized carbon emission factors, and this would require a collaboration of academia and industry.

Third, the carbon emissions produced in construction and maintenance stages of pedestrian bridges are estimated based on limited data available in literature. This method is adopted considering the relatively smaller fractions of carbon emissions of those two stages; that is, they are believed not to impact the final conclusions to a noticeable extent. However, such an estimation should be improved by using credible data regarding construction and maintenance. Again, this would require a

further investigation on construction method (i.e., construction equipment, energy consumption, building workers, etc.). The long-term maintenance, on the other hand, is to be detailed based on local construction environment (i.e., humidity, temperature, corrosive medium, etc.).

Last but not least, end-of-life decommissioning, as the last stage in the life-cycle of a structure, is not addressed in this work. This is due to the lack of universally-accepted decommissioning methods of FRP composites. Thermoset resin-based FRPs are known to have limited values in recycling, and thus, they are mostly dumped to landfills or sent to thermal power plants [84,85]. When reliable decommissioning method is established, a complete life-cycle analysis of carbon emissions can be conducted. As of today, all other stages, including material manufacturing, transportation, construction and maintenance, seem to favor the FRP composites over other materials.

6. Conclusions

In this work, three typical FRP composite structures were investigated in terms of their carbon emissions, including pedestrian bridges constructed with pultruded GFRP structural profiles, concrete structures reinforced by GFRP and CFRP rebars, and existing concrete and steel structures strengthened with CFRP sheets. When comparing to concrete and steel structures, FRP composite structures achieved equivalent structural performance with lighter weights, and more importantly, FRP structures generally exhibited reduced carbon emissions.

Direct carbon reductions were observed in three FRP structures. First, for simply-supported pedestrian bridges from 10 to 30 m, the total carbon emissions of FRP bridges are reduced by 66 % (STD = 10 %) and 77 % (STD = 9 %) as compared to steel and concrete bridges, respectively. Second, for reinforced concrete structures (i.e., concrete beams in this case) from 3 to 10 m, using CFRP rebars the average carbon reductions realized by equivalent stiffness and strength with steel rebars are 27 % (standard deviation, STD = 13 %) and 54 % (STD = 1 %), respectively; additionally, using GFRP rebars the average carbon reductions realized by equivalent stiffness and strength with steel rebars are 53 % (STD = 8 %) and 73 % (STD = 1 %) for all spans, respectively. Third, for strengthening of existing structures (i.e., concrete beams in this case) from 3 to 10 m, the average carbon reduction achieved by replacing steel plates by CFRP sheets is 72 % (STD = 6 %). It is noted that above calculations are based on available data of embodied carbon emissions of materials, and the observed dispersion within this type of data should be considered as a minor limitation of this work.

In addition, indirect carbon reductions were also discussed as the possible solutions for the field, including FRP reinforcement for concrete structures and FRP enclosure for houses. Durable FRP reinforcement could avoid the severe corrosion met by steel reinforcement in carbonized concrete, and FRP enclosure with a much lower thermal conductivity could promote the energy conservation. Both these two features of FRP composites may help reducing the carbon emissions in the long run, while future research is needed to provide quantified evidence.

In conclusion, FRP composite structures are believed to have great potential in realizing the carbon reduction and high performance in the field of civil engineering. In addition, in order to overcome the reported limitation, future work is needed to improve the evaluations regarding embodied carbon emissions of FRP composites as well as to clarify the carbon emissions occurred throughout the life-cycle of a structure.

CRedit authorship contribution statement

TianQiao Liu: Writing – original draft, Methodology, Investigation, Formal analysis, Funding acquisition. **Jun-Tian Tang:** Writing – original draft, Methodology, Investigation, Formal analysis. **Shaojie Zhang:** Writing – original draft, Methodology, Investigation, Formal analysis. **Li Dong:** Writing – original draft, Methodology, Investigation, Formal analysis. **Lili Hu:** Writing – original draft, Methodology, Investigation, Formal analysis. **Xinmiao Meng:** Methodology, Investigation. **Yange Zhao:** Methodology, Investigation. **Peng Feng:** Writing – review & editing, Supervision, Project administration, Methodology, Funding acquisition, Conceptualization.

Declaration of Competing Interest

The authors declare that they have no known competing financial interests or personal relationships that could have appeared to influence the work reported in this paper.

Data Availability

Data will be made available on request.

Acknowledgments

This work was supported by grants from National Key Research and Development Program of China (2023YFB3711600), National Natural Science Foundation of China (U2106219), Chongqing Construction Science and Technology Plan Project (Chengkezi2022No.2-1) and Natural Science Foundation of Chongqing (CSTB2023NSCQ-MSX0158).

Appendix A. Supporting information

Supplementary data associated with this article can be found in the online version at doi:10.1016/j.engstruct.2024.118482.

References

- [1] Hollaway LC. A review of the present and future utilisation of FRP composites in the civil infrastructure with reference to their important in-service properties. *Constr Build Mater* 2010;24(12):2419–45.
- [2] Liu TQ, Liu X, Feng P. A comprehensive review on mechanical properties of pultruded FRP composites subjected to long-term environmental effects. *Compos Part B Eng* 2020;191:107958.
- [3] Wang HT, Bian ZN, Chen MS, Hu L, Wu Q. Flexural strengthening of damaged steel beams with prestressed CFRP plates using a novel prestressing system. *Eng Struct* 2023;284:115953.
- [4] Yang JQ, Smith ST, Wang Z, Lim YY. Numerical simulation of FRP-strengthened RC slabs anchored with FRP anchors. *Constr Build Mater* 2018;172:735–50.
- [5] Yang JQ, Smith ST, Wang Z. Seismic behaviour of fibre-reinforced-polymer-and steel-strengthened timber connections. *Adv Struct Eng* 2019;22:502–18.
- [6] Yang JQ, Smith ST, Wu YF, Feng P. Strengthening single-bolt timber joints with externally bonded CFRP composites. *Structures* 2020;28:2671–85.
- [7] Yang JQ, Feng P, Liu B, Wang H, Zhao W, Hu L. Strengthening RC beams with mid-span supporting prestressed CFRP plates: an experimental investigation. *Eng Struct* 2022;272:115022.
- [8] Zhou W, Feng P, Lin H, Zhou P. Bond behavior between GFRP bars and coral aggregate concrete. *Compos Struct* 2022;306:116567.
- [9] Hu L, Feng P, Meng Y, Yang J. Buckling behavior analysis of prestressed CFRP-reinforced steel columns via FEM and ANN. *Eng Struct* 2021;245(5):112853.
- [10] Hu L, Liang X, Feng P, Li HT. Temperature effect on buckling behavior of prestressed CFRP-reinforced steel columns. *Thin-Walled Struct* 2023;188:110879.
- [11] Lin H, Zeng H, Feng P. Bond behavior of FRP-concrete wet-bonding interface under lateral confinement. *Eng Struct* 2023;292:116536.
- [12] Qin H, Liu TQ, Yu T, Yi S, Xiong J, Fan Y, et al. Application of ultra-lightweight and large-scale pultruded GFRP profile for external frame beam in high-rise buildings. *Compos Sci Eng* 2023;1:100–6 (In Chinese).
- [13] Worrell E, Price L, Martin N, Hendriks C, Meida LO. Carbon dioxide emissions from the global cement industry. *Annu Rev Energy Environ* 2011;26(1):303–29.
- [14] International Energy Agency (IEA). Energy Technology Perspectives 2020. Retrieved from: (www.iea.org) (2021/12/16).
- [15] Qianzhan Industrial Research Institute. China has become the largest cement producer and distributor in the world 2021. Retrieved from: (<https://bg.qianzhan.com/report/detail/300/210219-47d5e507.html>) (2022/6/12).
- [16] National Bureau of Statistics of China 2022. Retrieved from: (<https://data.stats.gov.cn/easyquery.htm?cn=A01>) (2022/6/12).
- [17] United Nations Framework Convention on Climate Change. Kyoto Protocol Reference Manual on Accounting of Emissions and Assigned Amount. United Nations 2009.
- [18] Xinhua News Agency. Presidential Address at the General Debate of the seventy-fifth Session of the United Nations General Assembly. Retrieved from: www.xinhuanet.com (2020/09/22).
- [19] EUR27666. Prospect for new guidance in the design of FRP (Ascione, L., Caron, J. F., Godonou, P., Van IJselmuiden, K., Knippers, J., Mottram, T., Oppe, M., Gantrris Sorensen, M., Taby, J., Tromp, L.), Publications Office of the European Union 2016.
- [20] Liu TQ, Feng P, Wu Y, Liao S, Meng X. Developing an innovative curved-pultruded large-scale GFRP arch beam. *Compos Struct* 2021;256:113111.
- [21] Liu T, Feng P, Lu X, Yang JQ, Wu Y. Flexural behavior of a novel hybrid multicell GFRP-concrete beam. *Compos Struct* 2020;250:112606.
- [22] Zhang C. The environmental impacts of fibre-reinforced polymer composites in construction. *Proc Inst Civ Eng-Const Mater* 2015;168(6):276–86.
- [23] Daniel RA. Environmental considerations to structural material selection for a bridge (Rotterdam) Eur Bridge Eng Conf, Lightweight Bridge Decks 2003 (Rotterdam).
- [24] Tanaka H, Tazawa H, Kurita M, Shimomura T. A case study on life-cycle assessment of environmental aspect of FRP structures (Miami, United States) Third Int Conf FRP Compos Civ Eng (CICE) 2006 (Miami, United States).
- [25] Dai JG, Ueda T. Carbon Footprint Analysis of Fibre Reinforced Polymer (FRP) Incorporated Pedestrian Bridges: A Case Study. In *Key Engineering Materials*, 517. Trans Tech Publications Ltd; 2012. p. 724–9.
- [26] Mara V, Haghani R. Upgrading bridges with fibre reinforced polymer decks—a sustainable solution. *Conf Civ Eng Infrastruct Based Polym Compos (CECOM)* 2012;1:79–80.

- [27] Mara V, Haghani R, Harryson P. Bridge decks of fibre reinforced polymer (FRP): a sustainable solution. *Constr Build Mater* 2014;50:190–9.
- [28] Li YF, Yu CC, Chen SY, Sainey B. The carbon footprint calculation of the GFRP pedestrian bridge at Tai-Jiang National Park. *Int Rev Spat Plan Sustain Dev* 2013;1(4):13–28.
- [29] Maxineasa SG, Isopescu DN, Entuc IS, Taranu N, Lupu LM, Hudisteanu I. Environmental performances of different carbon and glass fibre reinforced polymer shear strengthening solutions of linear reinforced concrete elements. *Bull Transilv Univ Brasov Eng Sci Ser I* 2018;11(3):107–15.
- [30] Maxineasa SG, Taranu N. Traditional building materials and fibre reinforced polymer composites. A sustainability approach in construction sector. *Buletinul Institutului Politehnic din Iasi. Sect Constr, Arhit* 2013;59(2):55.
- [31] Li Y.F., Yu C.C., Meda H.A. A Study of the Application of FRP Structural Members to the Green Fences. 3rd Annual International Conference on Architecture and Civil Engineering 2015.
- [32] Zubail A, Traidia A, Masulli M, Vatopoulos K, Villette T, Taie I. Carbon and energy footprint of nonmetallic composite pipes in onshore oil and gas flowlines. *J Clean Prod* 2021;305:127150.
- [33] Song YS, Youn JR, Gutowski TG. Life cycle energy analysis of fiber-reinforced composites. *Compos Part A Appl Sci Manuf* 2009;40(8):1257–65.
- [34] Joshi SV, Drzal LT, Mohanty AK, Arora S. Are natural fiber composites environmentally superior to glass fiber reinforced composites? *Compos Part A Appl Sci Manuf* 2004;35(3):371–6.
- [35] Vigneshwaran S, Sundarakannan R, John KM, Deepak Joel Johnson R, Arun Prasath K, Ajith S, et al. Recent advancement in the natural fiber polymer composites: a comprehensive review. *J Clean Prod* 2020;277:124109.
- [36] Chen C, Yang Y, Yu J, Tan H, Sui L, et al. Eco-friendly and mechanically reliable alternative to synthetic FRP in externally bonded strengthening of RC beams: natural FRP. *Compos Struct* 2020;241:112081.
- [37] Qureshi J, Mottram JT. Response of beam-to-column web cleated joints for FRP pultruded members. *J Compos Constr* 2014;18(2):04013039.
- [38] Al-Lami A, Hilmer P, Sinapius M. Eco-efficiency assessment of manufacturing carbon fiber reinforced polymers (CFRP) in aerospace industry. *Aerosp Sci Technol* 2018;79:669–78.
- [39] Önal M, Neşer G. Sustainability of the production of composite boat by life cycle management approach. "Micrea cel Batran. *Nav Acad Sci Bull* 2013;vol.XVI(issue 1).
- [40] Hammond G., Jones C. Inventory of carbon and energy (ICE). Bath: Sustainable Energy Research Team, Department of Mechanical Engineering, University of Bath 2008.
- [41] Hammond G., Jones C., Lowrie E.F., Tse P. Embodied carbon. The inventory of carbon and energy (ICE) 2011 Version 2.0.
- [42] Kara S., Manmek S. Composites: Calculating their Embodied Energy (CEE). Life Cycle Engineering and Management Research Group. University of New South Wales 2009.
- [43] Zhang C, Amaduddin M, Canning L. Carbon dioxide evaluation in a typical bridge deck replacement project. *Proc Inst Civ Eng-Energy* 2011;164(4):183–94.
- [44] GB/T-51366 2019. Building carbon emission calculation standard. Ministry of Housing and Urban-Rural Development 2019. (In Chinese).
- [45] T/CECS-692 2020. Technical specification for pultruded fiber reinforced polymer composites structure. China Association for Engineering Construction Standardization 2020. (In Chinese).
- [46] JTG-D64 2015. Specifications for design of highway steel bridge. Ministry of transportation and communications the People's Republic of China 2015. (In Chinese).
- [47] JTG-3362 2018. Specifications for design of highway reinforced concrete and prestressed concrete bridges and culverts. Ministry of transportation and communications the People's Republic of China 2018. (In Chinese).
- [48] CJJ-69 1995. Technical specifications of urban pedestrian overcrossing and underpass. Ministry of construction of the People's Republic of China 1995. (In Chinese).
- [49] GB-55001 2021. General code for engineering structure. Ministry of Housing and Urban-Rural Development of the People's Republic of China 2021. (In Chinese).
- [50] Liu TQ, Feng P, Bai Y, Bai S, Yang JQ, Zhao F. Flexural performance of curved-pultruded GFRP arch beams subjected to varying boundary conditions. *Eng Struct* 2024;308:117962.
- [51] Liu T. Stability behavior of pultruded glass-fiber reinforced polymer I-sections subject to flexure (Doctoral dissertation), University of Pittsburgh 2017.
- [52] Yang JQ, Liu TQ, Feng P. Enhancing flange local buckling strength of pultruded GFRP open-section beams. *Compos Struct* 2020;244:112313.
- [53] Liu TQ, Vieira JD, Harries KA. Predicting flange local buckling capacity of pultruded GFRP I-sections subject to flexure. *J Compos Constr* 2020;24(4):04020025.
- [54] Liu TQ, Yang JQ, Feng P, Harries KA. Determining rotational stiffness of flange-web junction of pultruded GFRP I-sections. *Compos Struct* 2020;236:111843.
- [55] Liu TQ, Vieira JD, Harries KA. Lateral torsional buckling and section distortion of pultruded GFRP I-sections subject to flexure. *Compos Struct* 2019;225:111151.
- [56] Liu TQ, Harries KA. Flange local buckling of pultruded GFRP box beams. *Compos Struct* 2018;189:463–72.
- [57] Kollár LP. Local buckling of fiber reinforced plastic composite structural members with open and closed cross sections. *J Struct Eng* 2003;129(11):1503–13.
- [58] GB-50010 2015. Code for design of concrete structures. Ministry of Housing and Urban-Rural Development of the People's Republic of China 2015. (In Chinese).
- [59] GB-50608 2020. Technical standard for fiber reinforced polymer (FRP) in construction. Ministry of Housing and Urban-Rural Development of the People's Republic of China 2020. (In Chinese).
- [60] Liu HB, Xiao ZG, Zhao XL, Al-Mahaidi R. Prediction of fatigue life for CFRP-strengthened steel plates. *Thin-Walled Struct* 2009;47(10):1069–77.
- [61] Ye L. Concrete Structure (Volume one). China Building Industry Press 2012. (In Chinese).
- [62] GB-50009 2012. Load code for the design of building structures. Ministry of Housing and Urban-Rural Development of the People's Republic of China 2012. (In Chinese).
- [63] American Association of State Highway and Transportation Officials. The Manual for Bridge Evaluation 2018. Washington, DC.
- [64] Imperator S, Rinaldi Z, Drago C. Degradation relationships for the mechanical properties of corroded steel rebars. *Constr Build Mater* 2017;148:219–30.
- [65] Vanama KR, Ramakrishnan B. Improved degradation relations for the tensile properties of naturally and artificially corroded steel rebars. *Constr Build Mater* 2020;249:118706.
- [66] GB-50367 2013. Code for design of strengthening concrete structure. Ministry of Housing and Urban-Rural Development of the People's Republic of China 2013. (In Chinese).
- [67] Arduini M, Nanni A. Behavior of precracked RC beams strengthened with carbon FRP sheets. *J Compos Constr* 1997;1(2):63–70.
- [68] Tavakkolizadeh M, Saadatmanesh H. Fatigue strength of steel girders strengthened with carbon fiber reinforced polymer patch. *J Struct Eng* 2003;129(2):186–96.
- [69] Wu G, Wang HT, Wu ZS, Ren Y. Experimental study on the fatigue behavior of steel beams strengthened with different fiber-reinforced composite plates. *J Compos Constr* 2012;16(2):127–37.
- [70] Wang HT, Bian ZN, Chen MS, Hu L, Wu Q. Flexural strengthening of damaged steel beams with prestressed CFRP plates using a novel prestressing system. *Eng Struct* 2023;284:115953.
- [71] GB-51367 2019. Standard for design of strengthening steel structure. Ministry of Housing and Urban-Rural Development of the People's Republic of China 2019. (In Chinese).
- [72] Hu L, Zhao XL, Feng P. Fatigue behavior of cracked high-strength steel plates strengthened by CFRP sheets. *J Compos Constr* 2016;20(6):04016043.
- [73] Hu L, Wang Y, Feng P, Wang H, Qiang H. Debonding development in cracked steel plates strengthened by CFRP laminates under fatigue loading: experimental and boundary element method analysis. *Thin-Walled Struct* 2021;166:108038.
- [74] Jena T, Kaewunruen S. Life Cycle Sustainability Assessments of an Innovative FRP Composite Footbridge. *Sustainability* 2021;13(23):13000.
- [75] Tan R. Analysis of Carbon Emission in Highway Bridge Construction. Master's thesis of Changsha University of Science and Technology 2017.
- [76] Xu S. The Research on Carbon Emissions of different structural materials in bridge life cycle, Master's thesis of Wuhan University of Technology 2012.
- [77] Zhang T. Research of low-carbon bridge evaluation system based on total life cycle. Master's thesis of China University of Mining and Technology 2018.
- [78] Qiu Q. A state-of-the-art review on the carbonation process in cementitious materials: fundamentals and characterization techniques. *Constr Build Mater* 2020; 247:118503.
- [79] Abdou OA, Murali K, Morsi A. Thermal performance evaluation of a prefabricated fiber-reinforced plastic building envelope system. *Energy Build* 1996;24(1):77–83.
- [80] Chowdhury E.U., Green M.F., Bisby L.A., Bénichou N., Kodur V.K.R. Thermal and mechanical characterization of fibre reinforced polymers, concrete, steel, and insulation materials for use in numerical fire endurance modelling. *Uneversi ondece documents etrouvedans: Structures under Extreme Loading, Proceedings of Protect, Whistler, BC* 2007.
- [81] International Organization for Standardization (ISO). Environmental management — Life cycle assessment — Principles and framework (ISO Standard No.14040 2006).
- [82] Chen C, Li X, Li C, Zhou Y, Sui L. Optimized flax FRP stirrup in reinforced concrete beam: Material property and shear performance. *Compos Struct* 2022;302:116219.
- [83] Zhou Y, Gong G, Xi B, Guo M, Xing F, Chen C. Sustainable lightweight engineered cementitious composites using limestone calcined clay cement (LC3). *Compos Part B: Eng* 2022;243:110183.
- [84] Conroy A, Halliwell S, Reynolds T. Composite recycling in the construction industry. *Compos Part A Appl Sci Manuf* 2006;37(8):1216–22.
- [85] Correia JR, Almeida NM, Figueira JR. Recycling of FRP composites: reusing fine GFRP waste in concrete mixtures. *J Clean Prod* 2011;19(15):1745–53.